Constraint Release in Entangled Binary Blends of Linear Polymers: A Molecular Dynamics Study

Zuowei Wang[†] **and Ronald G. Larson***

Department of Chemical Engineering, University of Michigan, Ann Arbor, Michigan 48109-2136

Received March 27, 2008; In Final Form May 3, 2008

ABSTRACT: We present extensive molecular dynamics simulations of the dynamics of diluted long probe chains entangled with a matrix of shorter chains. The chain lengths of both components are above the entanglement strand length, and the ratio of their lengths is varied over a wide range to cover the crossover from the chain reptation regime to tube Rouse motion regime of the long probe chains. Reducing the matrix chain length results in a faster decay of the dynamic structure factor of the probe chains, in good agreement with recent neutron spin echo experiments. The diffusion of the long chains, measured by the mean square displacements of the monomers and the centers of mass of the chains, demonstrates a systematic speed-up relative to the pure reptation behavior expected for monodisperse melts of sufficiently long polymers. On the other hand, the diffusion of the matrix chains is only weakly perturbed by the diluted long probe chains. The simulation results are qualitatively consistent with the theoretical predictions based on constraint release Rouse model, but a detailed comparison reveals the existence of a broad distribution of the disentanglement rates, which is partly confirmed by an analysis of the packing and diffusion of the matrix chains in the tube region of the probe chains. A coarse-grained simulation model based on the tube Rouse motion model with incorporation of the probability distribution of the tube segment jump rates is developed and shows results qualitatively consistent with the fine scale molecular dynamics simulations. However, we observe a breakdown in the tube Rouse model when the short chain length is decreased to around $N_S = 80$, which is roughly 3.5 times the entanglement spacing $N_e^P = 23$. The location of this transition may be sensitive to the chain bending potential used in our simulations.

1. Introduction

The dynamics of long linear polymer chains in a melt are dominated by entanglements between the densely interpenetrating and uncrossable molecules.[1–3] This collective many-body effect is represented in the tube or reptation model by an effective quadratic constraining potential acting on each monomer of the chain, which confines the chain within a tube-like region.[2,4] The monomer diffusion of an entangled chain is consequently predicted to undergo a transition from free three-dimensional Rouse motion with mean-square monomer displacement $g_1(t) \propto t^{1/2}$ at time scales shorter than the equilibration time τ_e to one-dimensional curvilinear reptation motion inside the confining tube, $g_1(t) \propto t^{1/4}$, above τ_e.[2,5] This Rouse-to-reptation transition has been verified in both neutron spin−echo (NSE) experiments[6] and computer simulations,[7–11] showing that the tube model qualitatively describes the dynamic properties of monodisperse entangled linear polymer melts. However, to provide quantitative predictions, additional relaxation mechanisms, such as contour length fluctuations (CLF) and constraint release (CR), need to be incorporated into the tube models.[2,3,5]

Contour length fluctuations are the fluctuations of the primitive path length (i.e., the length of the tube),[12–15] and constraint release describes the effect of the finite lifetime of the topological constraints, arising from the motion of the surrounding chains.[14–19] While CLF is a single-chain effect involving the stretching and contracting of the chain along the tube, CR is a many-chain effect strongly dependent on the polymer molecular weight distribution of the melt. The CR effect becomes more important in polydisperse melts where the rapid motion of the short chains releases the constraints on the long chains, allowing the latter to relax more rapidly than they could by their own reptation. There have been many experimental and theoretical investigations of the effects of constraint release on the dynamic properties of polydisperse polymer melts.[3,14–33] In particular, binary blends of monodisperse linear polymers have been widely used as the simplest model polydisperse system to test CR-related tube theories, since in a binary blend the constraint release time scale can be easily controlled by varying the molecular weight of the shorter polymers. The linear viscoelastic properties of such blends also have some distinctive features, such as two peaks in the frequency dependence of the loss modulus at certain blend compositions, the locations and heights of which allow one to compare theoretical predictions and experimental measurements.[14]

Constraint release events cause local reorganization of the confining tube, a process dynamically analogous to the Rouse motion of a polymer chain in dilute solutions. Thus the tube itself can be treated as a Rouse-like chain with elementary segment size equal to the tube diameter, which is the random walk step size of the primitive path, and a fundamental jump time proportional to the reptation time of the surrounding chains.[28,29] This model of "constraint release Rouse motion" has been generalized by Doi et al.[17] and Viovy et al.[18] to predict the dynamic behavior of binary mixtures of long and short linear monodisperse chains (with N_L and N_S monomers respectively). Regimes of terminal relaxation of the long chains depend on the Struglinski−Graessley parameter,[34] $r_{SG} \equiv N_L N_e^2/N_S^3$, which is proportional to the ratio of the reptation time of the long chain, $\tau_{d,L} = 3\tau_e(N_L/N_e)^3$, to the constraint release Rouse time, $\tau_{CR,L} = 3\tau_e(N_S/N_e)^3(N_L/N_e)^2$, of its confining tube, where N_e is the number of monomers in the entanglement strand. When the value of r_{SG} is smaller than order unity, both the theories of Doi et al. and Viovy et al. predict that the long chain reptates in an undilated bare tube. However, in case of $r_{SG} \geq 1$, where the long chain relaxation in the terminal regime is dominated by the tube Rouse motion, the two theoretical approaches differ in the assumption of how the long chain is constrained to a tube. Doi et al. proposed that constraint release leads the long chain to reptate in an enlarged or dilated tube, using the idea of "tube dilation" first introduced by Marrucci,[16] while Voivy et

* Corresponding author. E-mail: rlarson@umich.edu.
[†] E-mail: wangzw@umich.edu.

10.1021/ma800680b CCC: $40.75
Published on Web 06/14/2008

al. argued that the long chain always reptates in a bare tube of constant diameter as long as the length of the short chain $N_S > N_e$, and the undilated bare tube itself reptates in a "supertube" defined by the mutual entanglements of the long chains. In both works, the CLF effects and the distribution of the CR time scales are ignored, which limits the possible quantitative comparison of these predictions with experiments. The most detailed treatment of CR Rouse motion is the self-consistent theory developed by Rubinstein and Colby, where the mobilities of the Rouse tube segments, rather than taking on a single value related to the mean disentanglement time,[17,18,28,29] are assigned randomly according to a probability distribution determined from the tube survival relaxation spectrum, based on the solution of the single chain problem.[14] Likhtman and McLeish recently incorporated this approach into their tube theory together with the improved treatment of contour length fluctuations and the consideration of the longitudinal stress relaxation along the tube.[15] The self-consistent theories have been shown to provide reasonably good description of the experimental data on the viscoelastic properties of certain monodisperse[14,15] and binary blend samples.[14] In these calculations, the values of the tube segment mobilities are fixed after the initial assignment, while in reality the mobility of each segment might change from one jump to the next.[3]

The crossover from the chain reptation to the tube Rouse relaxation regimes with decrease of the short chain length has been qualitatively confirmed in tracer diffusion coefficient measurements[20,21,30] and viscoelastic experiments[22–25,34] on different binary blends. But the value of r_{SG} at the transitional point has been experimentally found to be smaller than the scaling-level argument of order unity.[19,20,25,35] Park and Larson estimated that this transitional value is at $r_{SG} \approx 0.064$.[19] Moreover they have shown that for cases of r_{SG} larger than this critical value the long chain reptation must be assumed to occur in a dilated tube to obtain agreement between their theoretical predictions based on an extension of the Milner-McLeish model[13] and the experimental results on the linear viscoelastic properties of binary blends of various polymers, even when the short chain length is much larger than the entanglement molecular weight.[19,35] The results imply that the transition from long chain reptation in a dilated to an undilated tube might not be simply defined by the condition that the short chain reaches a length of $N_S \approx N_e$.[18] Furthermore, the experiments of Watanabe et al. on the dielectric and stress relaxation in binary blends of linear polyisoprenes have suggested that the long chains can reptate in a partially dilated tube at times longer than the terminal time of the short chains, especially for systems with small r_{SG} values and low concentration of long chains.[25] These unsettled issues reflect that the CR Rouse tube models, though conceptually satisfactory, still need to be refined to describe the complete physical picture of constraint release. Hence investigations of the CR phenomenon on the molecular level have been sought to provide insights into some of these issues.

A direct experimental study of constraint release on the microscopic scale was carried out by Zamponi et al. via neutron spin echo spectroscopy on binary blends of a small fraction of labeled long chains in a shorter chain matrix.[26] The dynamic structure factor of the labeled chains was found to decay much faster with reduction of the matrix chain length, reflecting the more rapid loosening of the tube confinement due to the faster motion of the shorter surrounding chains. The time scales accessible by these NSE experiments are still below the reptation time of even quite short chains; thus the CR effects observed mainly resulted from the contour length fluctuations of the matrix chains. This demonstrates that the CLF alone can induce CR effects. Dynamic simulations using a slip-link model[36] have presented results consistent with these NSE experiments.[26] Since the fundamental time scales of constraint release events are generally considered to be related to the terminal time of the shorter chains, attaining a time window beyond the terminal relaxation regime of the shorter chains would be desirable for examining the CR Rouse motion models. Apart from the potential difficulties in NSE experiments, this objective could be realized in large scale computer simulations, which have been proved to be successful in validating the reptation model in mondisperse linear entangled melts[7–11] and the hierarchical relaxation model[37,38] in entangled branched polymers.[39]

There have been a number of simulation studies on concentrated polydisperse polymer systems, but the parameter ranges investigated have mostly fallen into either the nonentangled regime or the Rouse-reptation crossover region. Kolinski et al. performed Monte Carlo (MC) simulations on a cubic lattice to study the dynamics of a probe chain consisting 100 segments in a matrix of chain lengths varying from 50 to 800 segments.[40] The diffusion coefficient of the probe chain was found to decrease with increase of the matrix chain length, but no reptation behavior was observed, probably due to the use of a relatively low volume fraction of polymers. Baschnagel et al. employed the bond-fluctuation model to simulate bidisperse linear polymer melts, wherein the chain lengths were short enough to neglect entanglement effects.[41] The two components of the bidisperse melt were shown to have same static properties (end-to-end distance and radius of gyration), but different dynamic properties than their individual monodisperse melts. In the bidiperse case the mobility and relaxation rate of the short chains were reduced by the presence of the sluggish long chains, while the diffusion of the long chains were accelerated by the short species. Similar dynamic behavior has been observed in molecular dynamics (MD) simulations by Barsky on binary blends of linear flexible polymers with the longest chain length ($N = 90$) slightly above the entanglement strand length.[42] In those studies, the time dependence of the mean square displacement of the center of mass of the longest polymer chains showed a sublinear scaling behavior in the matrices with large enough short-chain lengths. Recently Lin et al. reported the dynamics of bidisperse polyethylene melts using a newly developed dynamic Monte Carlo algorithm on a high-coordination lattice.[43] Their melts were composed of one marginally entangled component and one unentangled component. The simulation results for the diffusion coefficients were found to be in reasonable agreement with theoretical models in the Rouse-reptation transitional region.[44–46]

Picu and Rakshit presented so far the only available simulation study on binary blends in the well-entangled region.[47] Their simulations were performed using a coarse-grained chain model which has been calibrated to reproduce the structure and dynamic properties of entangled monodisperse melts of linear flexible fine-grained bead-spring chains. The chain diffusion coefficients were investigated in binary blends where the short chains of weight fraction $\phi_S \geq 0.5$ (in most cases $\phi_S = 0.62$) are mixed with long chains and both types of chains are moderately to highly entangled. They showed that an increase of the chain length of one component reduces the diffusion coefficient of chains of the other component, but the influence of the long chain length on the diffusion of the short chains ceases if the length of the long ones is sufficiently large, which agrees with experiments. In this coarse-grained model, the constraint release effect is not incorporated. Thus the observed dynamic properties are attributed to the multibody interaction character of the end blobs of the model chains and to the contour length fluctuations.

In this work we perform extensive molecular dynamics simulations to investigate the dynamic properties of binary

blends of entangled linear semiflexible polymer chains. In our work, the lengths of the long chains $N_L \geq 350$ correspond to more than 15 entanglements using the entanglement length, $N_e^p = 23$, estimated from the primitive path analysis of monodisperse polymer melts employing the same chain model.[10] Since we are interested in the constraint release effects imposed by the short matrix chains on the long chain dynamics, the volume fraction of the long chains is kept at a low level of about 0.15 in most systems. The short matrix chain length N_S is decreased from N_L to a value slightly higher than one entanglement length. The value of the Struglinski−Graessley parameter is correspondingly increased from $r_{SG} = 0.0043$ to 11.85, transitioning from the chain reptation regime to the tube Rouse relaxation regime. Different dynamic properties are calculated and compared with available theoretical predictions and experimental data. The reminder of this paper is organized as following: In section 2, we give the details of the simulation model and the system parameters studied. The simulation results are presented and discussed in section 3, and the final conclusions are drawn in section 4.

2. Simulation Details

The linear polymers are represented by the bead-spring chain model used by Kremer and Grest in their simulations of monodisperse linear polymer melts.[7,8,48] In this model, all monomers interact via a truncated-shifted Lennard-Jones (LJ) potential

$$U_{LJ}(r) = \begin{cases} 4\varepsilon\left[\left(\frac{\sigma}{r}\right)^{12} - \left(\frac{\sigma}{r}\right)^{6} + \frac{1}{4}\right]; & r < r_c \\ 0; & r \geq r_c \end{cases} \quad (1)$$

where r is the distance between the centers of two monomers, and the cutoff radius r_c is taken to be $2^{1/6}\sigma$, yielding purely repulsive interactions between the monomers. The LJ parameter is set to be $\varepsilon = 1.0k_BT$ where k_B is the Boltzmann constant and T is the absolute temperature. The monomers of the same chain are connected to their sequential neighbors by the finite extensible nonlinear elastic (FENE) potential

$$U_{FENE}(r) = -\frac{1}{2}kR_0^2 \ln\left(1 - \frac{r^2}{R_0^2}\right), \quad (2)$$

where the spring constant is $k = 30\varepsilon/\sigma^2$ and the maximum bond length is $R_0 = 1.5\sigma$, at which the elastic energy of the bond becomes infinite. The combination of U_{LJ} and U_{FENE} leads to an average bond length $\langle l^2 \rangle^{1/2} = 0.97\sigma$. In addition, a three-bead bending potential is used to introduce bending stiffness into the polymer chain,

$$U_{bend}(\theta) = k_\theta(1 - \cos\theta), \quad (3)$$

where $\cos\theta_i = (\hat{\mathbf{r}}_i - \hat{\mathbf{r}}_{i-1}) \cdot (\hat{\mathbf{r}}_{i+1} - \hat{\mathbf{r}}_i)$, and $(\hat{\mathbf{r}}_i - \hat{\mathbf{r}}_{i-1})$ is the unit bond vector pointing from the center of monomer $i - 1$ to that of monomer i. The bending stiffness parameter is chosen to be $k_\theta = 2$, which leads to a semiflexible polymer with the characteristic ratio of $C_\infty = 3.4$ and the statistical segment length $b = C_\infty^{1/2} l = 1.79\sigma$. Primitive path analysis on the monodisperse melts consisting of the same type of semiflexible polymers yields an entanglement spacing of $N_e^p = 23$.[10]

The velocity Verlet algorithm is utilized to integrate the equations of motion of the monomers. The system is coupled to a Langevin thermostat by the standard equation,

$$m\ddot{\mathbf{r}}_i = -\nabla U(\mathbf{r}_i) - \Gamma\dot{\mathbf{r}}_i + \mathbf{W}_i(t) \quad (4)$$

where $\mathbf{r}_i$ is the coordinate of the ith monomer, m is the monomer mass, and Γ is the friction coefficient set to be $\Gamma = 0.5(mk_BT)^{1/2}/\sigma$. The stochastic force $\mathbf{W}_i$ is given by a δ-correlated Gaussian noise source. The simulations are performed in the NVT ensemble with periodic boundary conditions applied in all three dimensions of the cubic simulation box. The time step $\Delta t = 0.012\tau$ is used in all simulation runs, where $\tau = (m\sigma^2/k_BT)^{1/2}$ is the LJ time unit. The length and time scales in the systems are set by σ and τ, respectively.

The system parameters of the polymer melts we studied are listed in Table 1. The global number density of the chain segments is set to a fixed value of $\rho = 0.85\sigma^{-3}$ for all simulated systems.[7,48] In most cases, the long chain length is taken to be $N_L = 350$ with the number of entanglements per chain $Z_L = N_L/N_e^p = 15.2$. A few runs with $N_L = 500$ ($Z_L = 21.7$) are also performed to check for possible finite chain length effects. Starting from the monodisperse melt with $N = 350$, the length of the short matrix chains is gradually decreased to $N_S = 25$ ($Z_S = 1.1$) where the short chains themselves are marginally entangled. Correspondingly, the value of r_{SG} is varied by more than three decades, which should cover all chain reptation and tube Rouse relaxation regimes. In all binary blends we have $N_L \ll N_S^2$, so the long chains should not be swollen by the short chains, as confirmed in our simulations where we find that the average end-to-end distance and radius of gyration of the long chains remain nearly constant irrespective of the change in N_S.

The number fraction of the long chain segments n_L is defined as the ratio of the total number of the long chain segments divided by the total number of chain segments in the system, i.e., $n_L = M_L \times (N_L - 1)/[M_L \times (N_L - 1) + M_S \times (N_S - 1)]$. The number density of the long chain segments ρ_L is thus simply given by $\rho_L = \rho n_L$. In the current work, we focus on investigating constraint release effects arising from the motion of the short matrix chains on the relaxation of the long chains, leaving the problem of mutual entanglement effects between the long chains and the possible formation of "supertube" for later study. Thus the density of the long chains is kept rather low but still large enough to provide sufficient statistics with affordable computational efforts. Taking the binary blend as a semidilute solution of the long chains in Θ-condition, we can estimate the entanglement length between the long chains, $N_e(\phi_L) = N_e(1)\phi_L^{-4/3}$, with ϕ_L being the volume fraction of the long chain segments.[5] Using $N_e(1) = 23$ and the relative volume fraction of $\phi_L = 0.15$ ($n_L = 0.15$), one gets $N_e(0.15) \approx 289$, which is slightly below the long chain length of $N_L = 350$. We have examined the possible entanglement effects between the long chains by increasing the long chain segment fraction from $n_L = 0.15$ to 0.20 for the binary blends with $N_L = 350$ and $N_S = 80$. Although the effective entanglement length between the long chains is thereby reduced from $N_e(0.15) \approx 289$ to $N_e(0.20) \approx 197$, the simulation results show nearly no difference. Thus no strong entanglements between the long chains or the formation of a "supertube" is expected in the range of parameters investigated in the current work. The long chain density we studied is comparable with that used in the NSE experiments ($\phi_L = 0.05$)[26] and the tracer diffusion measurements ($\phi_L < 0.1$).[21]

The initial configurations of the monodisperse and bidisperse polymer melts are generated using the equilibration method developed by Auhl et al.,[48] which was later generalized by Zhou and Larson to prepare the initial configurations of asymmetric star polymer melts.[39] The details of this method could be found in these two papers.[39,48] In brief, a polymer melt system of 500 chains each having 100 monomers is first equilibrated through the MD algorithm described above. The equilibrated chains are then cut into halves to construct a database of 1000 building block chains each composed of 50 monomers. We then randomly pick up building blocks from the database and link them end-to-end into linear chains of the desired length. If the

produced chain length is longer than the required value of N_L or N_S, which might not necessarily be an integral multiple of 50, the extra monomers are eliminated from one end of the chain. With the prepacking and slow push-off algorithm, the polymer melt is obtained by packing the newly generated chains into a simulation box, rearranging them to maximize the homogeneity in the monomer number density, and then gradually introducing the interchain excluded volume interactions.[48] The equilibration of the chain conformations is monitored by measuring the mean square internal distance $\langle R^2(n)/n\rangle$ with $n = |i-j|$ being the chemical distance. After that, a full MD simulation run for a time of $4.8 \times 10^4\tau$ is conducted to relax the configuration on short length scales.

The dynamic properties of the polymer melts are then calculated from MD simulation runs of duration $6-10 \times 10^5\tau$ (see Table 1). In this work, the monomer coordinates are corrected by subtracting the center of mass motion of the whole system before physical quantities are computed to correct for the drift.[8] For most of the binary blend systems, two individual runs, starting from different initial configurations, are performed in order to make sure that no finite size effect results from the limited number of the long probe chains. The two independent runs are found to produce very consistent results for all the physical quantities we are interested in, and the simulation data presented in this paper are the final results averaged over the two runs. We have also tested the possible system size effect, caused by the limited total number of chains in the simulation box, by varying the number of chains from $M = 100$ to 400 for the monodisperse melt of chain length $N = 80$. All results obtained at different M values are within statistical error bars, showing that our simulation systems (Table 1) are sufficiently large.

3. Results and Discussion

3.1. Dynamic Structure Factor. The dynamic structure factor of a single polymer chain is defined as[2]

$$S(k,t) = \frac{1}{N}\sum_{i,j}\langle \exp[i\mathbf{k}\cdot(\mathbf{r}_i(t) - \mathbf{r}_j(0))]\rangle, \quad (5)$$

which is a Fourier transform of the real-space pair correlation function $g(r,t)$. Here $\mathbf{k}$ is the wavevector and N is the number of monomers of the chain. The measurements of $S(k,t)$ in the NSE experiments have provided microscopic evidence for the reptation behavior[49] as well as the contour length fluctuation[50] and constraint release[26] effects in linear polymer melts. We can map our bead-spring chain model onto the polyethylene (PE) polymers studied in these NSE experiments by using the model-independent entanglement length N_e^P. The long, labeled, PE chains in the binary blends studied in NSE measurements have a molecular weight of $M_w = 36$ kg/mol (number of monomers $N^{PE} = 2570$).[26] According to the estimated tube diameter of $d = 46$ Å (corresponding to an entanglement length of $N_e^{NSE} \approx 160$),[49,51] the number of entanglements $Z^{PE} \approx 16$ of the long PE chain is very close to that of our bead-spring chain with $N_L = 350$ monomers for which $Z_L = 15.2$.

3.1.1. Monodisperse Melt. Neglecting the free Rouse motion of the monomers at early times $t < \tau_e$, the dynamic structure factor of a reptating chain can be calculated in the long chain limit as[49,52,53]

$$\frac{S(k,t)}{S(k,0)} = [1 - \exp(-k^2d_T^2/36)]S^{loc}(k,t) + \exp(-k^2d_T^2/36)S^{esc}(k,t) \quad (6)$$

where $S^{loc}(k,t)$ and $S^{esc}(k,t)$ are the contributions from the chain reptation inside the tube (local reptation at times $\tau_e < t < \tau_R$) and the escape of the chain out of its initial tube via reptation (up to the terminal time τ_d), respectively. d_T is the effective tube diameter, and τ_R is the Rouse time of the chain. The local reptation contribution was first given by de Gennes,[52]

$$S^{loc}(k,t) = \exp(t/\tau_o)erfc(\sqrt{t/\tau_o}), \quad (7)$$

where $\tau_o = 12/Wb^4k^4$ and b is the statistical segment length. To be consistent with previous simulation works,[9,11] the Rouse rate is defined as $W = k_BT/\zeta b^2$ with ζ being the effective monomer friction coefficient, which differs by a prefactor of 3 from that used in the NSE papers, $W = 3k_BT/\zeta b^2$.[49,53]

The exact expression for the escape term, $S_{rep}^{esc}(k,t)$, due to pure reptation, ignoring any internal dynamics of the chain, was given by Doi and Edwards.[2] In case of $qR_g \gg 2\pi$ where R_g is the radius of gyration of the chain, it can be approximated by[9,49]

$$S_{rep}^{esc}(k,t) = \frac{8}{\pi^2}\sum_{p=1,odd}^{\infty}\frac{1}{p^2}\exp(-p^2t/\tau_d), \quad (8)$$

where the terminal or reptation time is given by $\tau_d = N^3b^2/\pi^2Wd_T^2$. For time scales shorter than the Rouse time τ_R, it has been shown that the effect of reptation on the tube evacuation process is negligible in comparison to contour length fluctuations.[15] In this regime the fraction of monomers that have escaped from the initial tube due to CLF has a power law time-dependency, $\Psi(t) = 1.5(t/\tau_e)^{1/4}/Z$, where Z is the number of entanglements of the chain. An analytical expression for the escape term of the structure factor has been derived by incorporating this CLF effect,[53]

$$S_{CLF}^{esc}(k,t) = A[2\mu + e^{-2\mu} + 2 - 4\mu s(t) - 4e^{-2\mu s(t)} + e^{-4\mu s(t)}] \quad (9)$$

where $A = 1/S_{CLF}^{esc}(k,0)$ is the normalization factor,[50] $\mu = k^2Nb^2/12$, and $s(t) = \Psi(t)/2$ by assuming that after time t the number of monomers released from the tube is the same for each end of the chain.

We start our calculation of the single-chain dynamic structure factor with a monodisperse linear polymer melt of chain length $N = 350$. As has been done in previous MD simulations[54] and NSE experiments,[50] we calculate $S(k,t)$ both for the entire polymer chain with all 350 monomers and for only the central 200 monomers of the chain in order to separate the contour length fluctuations from the chain reptation. In the later case, the first 75 monomers at each chain end are not taken into account. For a time scale up to $t = 60\,000\tau$, the maximum number of monomers released by CLF from the tube is estimated to be $350 \times \Psi(60000)/2 \approx 39$ on each side of the chain, where an equilibration time of $\tau_e = 2290\tau$ is used as determined in section 3.2.1. Thus in such a time window, the central part of the chain with 200 monomers feels only very weak contour length fluctuation effects and its dynamic structure factor should be very close to that of an infinitely long chain.

The normalized dynamic structure factor $S(k,t)/S(k,0)$ of the monodisperse polymer melt is plotted in Figure 1 as a function of time for different k values. In each case, the $S(k,t)$ curve drops quickly at early times and then slows down to approach a plateau at longer times, signifying the transition from the initial free Rouse-like motion to reptation. As expected from the effect of contour length fluctuations, the dynamic structure factor obtained from the whole chain shows a stronger decay with time than that of the central part of the chain.[50,54] To compare with the theoretical predictions, we take the Rouse rate $W = 6.24 \times 10^{-3}\tau^{-1}$ (see section 3.2.1) and use the tube diameter d_T as the only fitting parameter. The data obtained from the subchain of central 200 monomers are fitted with the pure reptation model by employing $S_{rep}^{esc}(k,t)$ (eq 8) in eq 6. Even though the k values studied in Figure 1 are in the vicinity of $kR_g \approx 2\pi$, the use of the approximate formula of eq 8 for the escape contribution is good enough to provide a satisfactory description of the simulation results with a tube diameter of $d_T = 10.3\sigma$. When

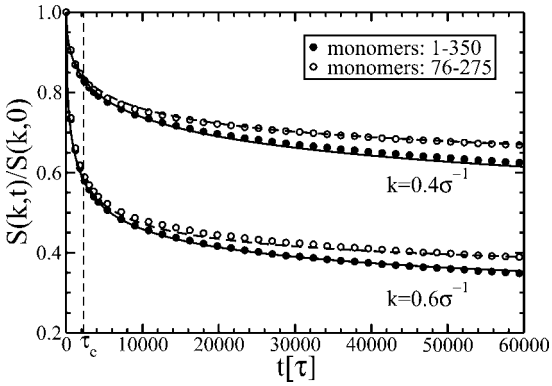

Figure 1. Single-chain dynamic structure factor $S(k,t)$ of the monodisperse linear polymer melt with chain length $N = 350$ for various k values. The lines are fits to the theoretical predictions of the pure reptation model using eqs 6 and 8 (dashed) and the model with consideration of contour length fluctuations using eqs 6 and 9 (solid), respectively. The fitting parameters are the tube diameters $d_T = 10.3\sigma$ for the dashed lines and $d_T = 9.9\sigma$ for the solid lines.

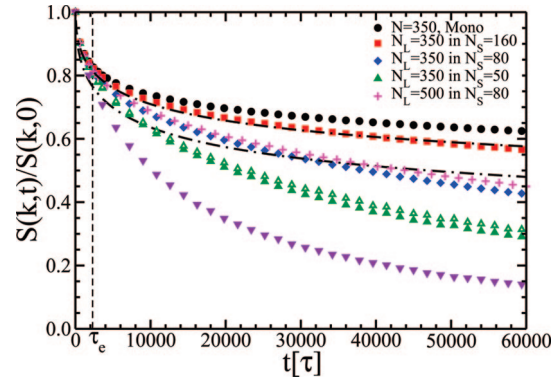

Figure 2. Single-chain dynamic structure factor $S(k, t)$ of the long probe chains in binary blends at $k = 0.4\sigma^{-1}$. The filled (and plus) symbols correspond to the results calculated for the entire probe chain with all $N_L = 350$ (or 500) monomers, and the open ones are calculated for the central 200 monomers of the probe chain. Since the relative difference between the two sets of data are very similar for all binary blends, only the data obtained from the system with $N_S = 50$ (open triangle-up) in the latter case are shown for simplicity. The data points for the monodisperse melt are the same as that in Figure 1. The number fraction of the long chain segments is $n_L \approx 0.15$ in all binary blends. The dotted-dashed lines are the theoretical predictions using the model with consideration of CLF (eqs 6 and 9) for a probe chain with 350 monomers using tube diameters $d_T = 10.7\sigma$ (upper) and 12.7σ (lower), respectively.

the CLF effect is of concern, the prediction of eq 9 in combination with eq 6 describes the calculation data for the whole chain very well, giving a tube diameter of $d_T = 9.9\sigma$, which is slightly smaller than that of the asymptotically long chain (10.3σ). The good agreement between the simulation and theoretical results in Figure 1 not only validates the tube model in predicting the dynamic structure factors of entangled linear polymer chains but also indicates that at short time scales constraint release has negligible effect on the dynamics of monodisperse polymer melts of sufficiently long chains.

Taking the entanglement strand to be a random walk with size $d_T^2 = N_e b^2$, the entanglement length calculated from the fitted values of the tube diameter is about $N_e = 32 \pm 2$, which is larger than the value of $N_e^p = 23$ ($d_T^p = 8.6\sigma$) determined from the primitive path analysis.[10] The plateau modulus measurements or rheological simulations on the melt systems of the same semiflexible chains are currently not available, but they are supposed to provide similar tube diameter or entanglement length as the primitive path analysis.[10] The overestimation of the tube diameter from dynamic structure factor calculations has also been found in the MD simulations of flexible entangled chains of $N = 700$ monomers, where this is attributed to the finite chain length.[9,54] But the NSE experiments on PE chains, which show no significant chain length dependence, also provide a tube diameter ($d = 46$ Å) somewhat larger than that deduced from the plateau modulus measurements ($d = 42$ Å).[49,55]

3.1.2. Binary Blends. Figure 2 presents the simulation results on the dynamic structure factor of the long probe chains in binary blends with various short matrix chains for $k = 0.4\sigma^{-1}$. The results on $S(k,t)$ calculated for other k values show qualitatively the same behavior. In Figure 2, the number fraction of the long chain segments is kept to be the same ($n_L \approx 0.15$, see Table 1) for all the binary blends. We have increased n_L from 0.15 to 0.20 for the case of $N_L = 350$ and $N_S = 80$, and found a small increase of the $S(k,t)/S(k,0)$ values at longer times with a maximum 4% difference at $t = 60\,000\tau$ for $k = 0.4\sigma^{-1}$. This means that the concentration of the long chains we studied is still in the dilute regime and little mutual entanglement between the long chains occurs. Figure 2 also reveals that the dependence of the dynamic structure factor on the length of the long probe chains is rather weak for our semiflexible linear chains in comparison with that of flexible linear chains in the same chain length range.[9,54] This is mainly due to the larger number of entanglements obtained for the semiflexible chains. In the same matrix of chain length $N_S = 80$, the structure factor of the $N_L = 500$ probe chain is only slightly larger than that of the chain with $N_L = 350$ for $k = 0.4\sigma^{-1}$ (compare the plus and diamond symbols in Figure 2) but is nearly coincident with the later one for $k = 0.6\sigma^{-1}$ (not shown). The diffusion behavior of these long probe chains has also been found to have a very weak N_L dependence at short to intermediate time scales.

The faster decay of $S(k,t)$ with decreasing matrix chain length in Figure 2 clearly reveals the increased loosening of the tube confinement due to the enhanced constraint release effect and is in good agreement with that observed in the NSE experiments on binary blends of PE polymers.[26] The CR effect becomes evident even when the matrix chain length is half of the long chain length ($N_S = 160$ and $N_L = 350$), corresponding to a Struglinski−Graessley parameter of $r_{SG} = 0.0452$, which is much smaller than unity but close to the transitional value estimated by Park and Larson ($r_{SG} \approx 0.064$).[19] More importantly, the $S(k,t)$ curves of the long probe chains in binary blends

Table 1. System Parameters: Number of Chains M, Number of Monomers Per Chain N, Number of Entanglements Per Chain Z Calculated Using the Entanglement Length of $N_e^p = 23$,[10] Struglinski−Graessley Parameter r_{SG}, Long Chain Segment Number Fraction n_L, Long Chain Segment Number Density ρ_L, and Total MD Simulation Time t_{tot} Performed in the Equilibrium Runs

$N_L \times M_L$	$N_S \times M_S$	Z_L	Z_S	r_{SG}	n_L	$\rho_L(\sigma^{-3})$	$t_{tot}(\tau)$
350 × 200	-	15.2	-	0.0043	1.0	0.850	1.0×10^6
350 × 30	160 × 375	15.2	7.0	0.0452	0.149	0.127	1.0×10^6
350 × 30	120 × 500	15.2	5.2	0.1071	0.150	0.128	7.0×10^5
350 × 30	80 × 750	15.2	3.5	0.3616	0.150	0.128	1.0×10^6
350 × 40	80 × 700	15.2	3.5	0.3616	0.202	0.172	1.0×10^6
500 × 36	80 × 1275	21.7	3.5	0.5166	0.151	0.128	6.0×10^5
350 × 30	50 × 1200	15.2	2.2	1.4812	0.151	0.128	9.0×10^5
350 × 30	25 × 2400	15.2	1.1	11.849	0.154	0.131	7.0×10^5

Table 2. Terminal Time $\tau_{d,S}$, Plateau Values of the Mean Square Monomer Displacement $g_{2,S}^p$ and Mean Square Radii of Gyration $R_{g,S}^2$ of the Short Matrix Chains.

N_S	$\tau_{d,S}$ ($\times 10^4\tau$)	$g_{2,S}^p$ (σ^2)	$R_{g,S}^2$ (σ^2)
160	36.0 ± 1.0	81.4	84.7
120	13.6 ± 1.0	59.5	63.2
80	4.6 ± 0.1	38.6	41.1
50	1.4 ± 0.1	22.5	24.6
25	0.45 ± 0.02	9.9	11.2

deviate from that of the monodisperse polymer melt immediately after the equilibration time τ_e, rather than at the time conjectured theoretically, which is the terminal time of the short chains $\tau_{d,S}$. This could be a result of the broad distribution of the lifetimes of the topological constraints. For a given probe chain, the segments of the surrounding short chains, which effectively contribute to creation of the confining tube, could be localized anywhere along their backbones. Those close to the chain ends could move away quickly from the tube region due to contour length fluctuations, releasing the constraint or entanglement at short time scales.[26] On the other hand, an entanglement in the middle part of the short chains can only be released by reptation of these chains. As a result, although the mean lifetime of the topological constraints is related to $\tau_{d,S}$, constraint release occurs at all time scales with a broad probability distribution. The reduction of the matrix chain length not only introduces a smaller value of $\tau_{d,S}$, but also a higher concentration of matrix chain ends for a fixed monomer density. Thus, the dynamic relaxation of the probe chains in a matrix of shorter chains is faster than that in a relatively longer chain matrix over the whole time range above the equilibration time τ_e.

Similar to the monodisperse case in Figure 1, the dynamic structure factor in binary blends is also calculated for both the entire probe chain and the central part of the chain, neglecting 75 monomers at each end. Although the absolute difference between the two sets of data becomes slightly smaller with a decrease of the matrix chain length, the relative difference remains almost constant in all cases. At time $t = 60\,000\tau$, the relative difference between the two $S(k,t)/S(k,0)$ values is about 7.5% for $k = 0.4\sigma^{-1}$ (compare the filled and open triangle-up symbols in Figure 2) and about 13% for $k = 0.6\sigma^{-1}$. This reflects that the constraint release events are affecting the relaxation of the probe chain relatively uniformly along the entire chain.

An attempt to fit the simulation data for $S(k,t)$ with the theoretical predictions given above (eqs 6 and 9) has failed for all the binary blends, owing to the neglect of the constraint release effect in the theoretical models. In Figure 2, we plot the analytical predictions of the model with consideration of CLF effects (eqs 6, 7,and 9) for the structure factor of an entangled chain with 350 monomers. With decrease of the short matrix chain length, a larger tube diameter has to be used in the theoretical calculation to predict results comparable to the simulation data calculated for the entire chain. Even so, the theoretical and simulation curves show a mismatch over the whole time range studied in Figure 2. A similar discrepancy is also observed between the prediction of the pure reptation model (eqs 6, 7,and 8) and the simulation $S(k,t)$ data calculated for the central part of the chain. To get an accurate theoretical description of the dynamic structure factor of polydisperse polymer melts, the constraint release effect, together with the broad lifetime distribution of the topological constraints, must be taken into account, as has been done in the self-consistent theoretical model for predicting the linear viscoelasticity of binary blends.[14] The faster decay of the dynamic structure factor with decreasing matrix chain length could also be considered as an effective widening, or dynamic dilution, of the tube confining the long probe chain.[16] But there is still no analytical formula based on the tube dilation concept for the dynamic structure factor of polydisperse melts to which we could compare our simulation results. In addition, a direct quantitative comparison between our simulation data and the NSE experimental results[26] is also not straightforward, because the length ratios of the probe and matrix chains are not the same in the two cases and there is no exact mapping of our semiflexible bead-spring model chain with the PE polymers on the monomer level, due to differences in flexibility of the simulated chains and the experimental PE chains. Still a very good qualitative agreement is found between our Figure 1 and Figure 2 in Zamponi et al.'s paper for PE chains.[26]

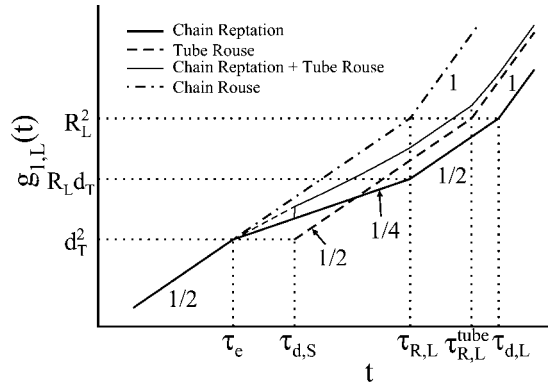

Figure 3. Schematic plot of the mean square monomer displacement $g_{1,L}(t)$ of the probe chain due to chain reptation, $g_{1,L}^{rep}$, (eq 10, thick solid line) and tube Rouse motion, $g_{1,L}^{tube}$, (eq 11, thick dashed line). The thin solid line is obtained by combining the reptation and tube Rouse motion contributions, see eq 13. The prediction for $g_{1,L}(t)$ of a free Rouse chain (dotted-dashed line) is also given for comparison.

3.2. Diffusion. In the theoretical treatments of entangled binary blends, the terminal time of the short matrix chains is generally taken as the characteristic time after which the constraint release effect dominates the dynamic relaxation of the long probe chains. To examine the dynamics beyond this time, we extend our MD simulations to time scales far beyond the terminal time of the short chains and analyze the diffusion of the monomers as well as the whole polymer chains to get a more direct comparison with the predictions of the constraint release Rouse model.[17,18]

3.2.1. Monomer Diffusion. The pure reptation model predicts that the mean square displacement of the monomers of an entangled polymer chain, $g_1(t) = \langle(\mathbf{r}_i(t) - \mathbf{r}_i(0))^2\rangle$, obeys the following power laws for various time regimes, as illustrated by the thick solid line in Figure 3:[2,9,15]

$$g_1^{rep}(t) = \begin{cases} 2\sqrt{\frac{3}{\pi}}b^2(Wt)^{1/2}, & t \lesssim \tau_e \\ \left(\frac{4}{3\pi}\right)^{1/4} bd_T(Wt)^{1/4}, & \tau_e \lesssim t \lesssim \tau_R \\ \sqrt{\frac{2}{N}}bd_T(Wt)^{1/2}, & \tau_R \lesssim t \lesssim \tau_d \\ 2\frac{d_T^2}{N^2}Wt, & \tau_d \lesssim t \end{cases} \quad (10)$$

where $W = k_BT/\zeta b^2$ is the Rouse monomer diffusion rate and d_T is the effective tube diameter. The equilibration time, Rouse time, and terminal (disengagement) time are defined in the tube model as $\tau_e = N_e^2/3\pi^2W$, $\tau_R = Z^2\tau_e$, and $\tau_d = 3Z\tau_R$, respectively, where Z is the number of entanglements $Z = N/N_e$. The mean square monomer displacement relative to the center of mass of the chain $\mathbf{R}$, $g_2 = \langle(\mathbf{r}_i(t) - \mathbf{R}(t) - \mathbf{r}_i(0) + \mathbf{R}(0))^2\rangle$, is expected to have the similar behavior as g_1 below the terminal time τ_d but to reach a plateau value equal to the mean square radius of gyration of the chain $R_g^2(N)$ for $t > \tau_d$.[9]

The simulation results for $g_1(t)$ and $g_2(t)$ of the monodisperse melt are plotted in Figure 4 as the circles. These data are obtained by averaging over the innermost six monomers of each chain to avoid the influence of the rapidly moving chain ends.[8,9] The first three power laws below τ_d predicted in eq 10 are clearly recovered by the simulation data, confirming that the semiflexible chains with $N_L = 350$ monomers are long enough to display reptation behavior. A power law fit to the free Rouse motion regime at early times, $g_1(t) = 0.494(5)(t/\tau)^{1/2}\sigma^2$, yields the Rouse

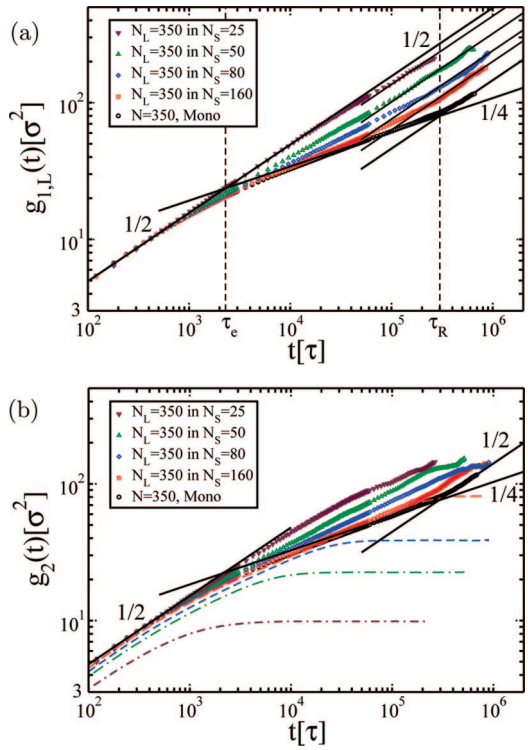

Figure 4. Mean square monomer displacement $g_{1,L}(t)$ (a) and $g_{2,L}(t)$ (b) of the long probe chain with 350 monomers in binary blends with various short matrix chains. The mean square monomer displacements $g_{2,S}$ of the short chains are also given in (b) for $N_S = 160$ (long-dashed line), $N_S = 80$ (short-dashed line), $N_S = 50$ (long-dotted-dashed line), and $N_S = 25$ (short-dotted-dashed line). All results are averaged over the innermost six monomers of the chain.

rate $W = 6.24 \times 10^{-3}\tau^{-1}$. The first crossover point, between the $g_1 \propto t^{1/2}$ and $g_1 \propto t^{1/4}$ power law regimes, gives an estimation of the equilibration time $\tau_e = 2290 \pm 100\tau$, which is larger than that given by a previous MD simulation ($\tau_e = 1800 \pm 100\tau$) on the same kind of semiflexible polymer melt but using shorter chains in a smaller simulation box.[11] The entanglement strand length is consequently estimated to be $N'_e = (3\pi^2 W\tau_e)^{1/2} = 21 \pm 2$ (or an effective tube diameter $d'_T = 8.1 \pm 0.4\sigma$). This value of N'_e is smaller than that determined by the primitive path analysis ($N_e^P = 23$)[10] and by the above theoretical fit to the dynamic structure factor ($N_e = 32$). A similar dependence of the N_e value on the methods of obtaining it has been observed in the MD simulations of Pütz et al. for linear flexible polymer chains.[9] The second crossover point, from the $g_1 \propto t^{1/4}$ power law to $g_1 \propto t^{1/2}$, corresponds to the Rouse time τ_R, above which all monomers participate in coherent motion of the chain along the tube, which is reptation motion. Figure 4 provides a value of $\tau_R = (3.0 \pm 0.3) \times 10^5\tau$ for the chain with 350 monomers, yielding an entanglement length of $N''_e = N/(\tau_R/\tau_e)^{1/2} = 31 \pm 2$ that is larger than N'_e determined from the first crossover point. This increase in the values of N_e between the first and second crossover points has been interpreted as a time-dependent widening of the confining tube experienced by the probe chain.[11] The $g_2(t)$ data in Figure 4b show the same qualitative behavior as $g_1(t)$ but are of lower values than $g_1(t)$, due to the subtraction of the center of mass motion of the whole chain. The equilibration time and Rouse time inferred from the $g_2(t)$ curve are $\tau_e = 2160 \pm 100\tau$ and $\tau_R = (2.9 \pm 0.3) \times 10^5\tau$, respectively, consistent with those obtained from $g_1(t)$. In the current paper, we generally use physical quantities, such as τ_e and τ_R, determined from the $g_1(t)$ results for our discussions, unless otherwise stated.

In binary blends, constraint release events due to rapid motion of the short matrix chains cause reorganization of the confining tube of the long probe chain. The theoretical work of Viovy et al., based on the concept of constraint release Rouse motion, predicts the mean square displacement of a tube segment of size d_T as (thick dashed line in Figure 3)[18]

$$g_{1,L}^{tube}(t) \cong \begin{cases} d_T^2(t/\tau_{obs})^{1/2}, & \tau_{obs} \lesssim t \lesssim \tau_R^{tube} \\ d_T^2 Z_L t/\tau_{R,L}^{tube}, & \tau_R^{tube} \lesssim t \end{cases} \quad (11)$$

with the Rouse time of the tube given by

$$\tau_{R,L}^{tube} \approx \tau_{obs} Z_L^2, \quad (12)$$

τ_{obs} is the fundamental jump time of the tube segment and is taken to be comparable to the terminal relaxation time $\tau_{d,S}$ of the short matrix chains, i.e., $\tau_{obs} \approx \tau_{d,S}$. The CR effect becomes important when the tube Rouse time $\tau_{R,L}^{tube}$ is shorter than the reptation or terminal time $\tau_{d,L}$ of the long probe chains. If the chain reptation and tube Rouse motion processes are assumed to be independent, the net mean square monomer displacement of the long probe chain is

$$g_{1,L}(t) \cong g_{1,L}^{rep}(t) + g_{1,L}^{tube}(t) \quad (13)$$

which is sketched in Figure 3 as the thin solid line. In the CR Rouse model, the contour length fluctuations of the short matrix chains have been neglected; thus no contribution from constraint release is considered at time scales shorter than $\tau_{d,S}$. In that regime ($t \leq \tau_{d,S}$) the theoretical $g_{1,L}(t)$ curve follows the pure reptation behavior (thick solid line). The NSE experiments and our simulations of the dynamic structure factor have revealed that the CR events happen already at early times starting at τ_e, so the monomer diffusion curve would more likely follow the thin dashed line in the time region between τ_e and $\tau_{d,S}$, rather than exhibit a sudden jump at $\tau_{d,S}$.

Figure 4 presents our simulation results for $g_{1,L}(t)$ and $g_{2,L}(t)$ of the long probe chains with $N_L = 350$ monomers in various short chain matrices. For comparison, the $g_{2,S}(t)$ curves of the matrix chains are also given in Figure 4b. In all cases, the results are averaged over the innermost six monomers of each chain. At short time scales the monomers diffuse by free Rouse motion without feeling the tube confinement. The $g_{1,L}(t)$ and $g_{2,L}(t)$ curves of all systems follow the same universal scaling law of $g_{1(2)} \propto t^{1/2}$ and fall exactly on top of each other. The onset of the slowing down of the monomer diffusion in binary blends occurs at the same time as that in the monodisperse system. This means that the equilibration time τ_e is a general physical quantity only determined by the chain model used in the simulations but independent of the chain length distribution. However, the diffusion of the long probe chains at longer time scales is strongly affected by the length of the matrix chains due to the constraint release effect.

Since the CR effect is theoretically assumed to become effective at the time scale $\tau_{d,S}$, we first give an estimation of the terminal time of the matrix chains by using the $g_{2,S}(t)$ results in Figure 4b. The matrix chains we studied are relatively short, and so it is somewhat difficult to distinguish the second $t^{1/2}$ power law regime in their monomer diffusion curves.[9,11] We thus take the onset time of the plateau regime of the $g_{2,S}(t)$ curves as an estimation of $\tau_{d,S}$ instead of using the crossover between the $g_{2,S} \propto t^{1/2}$ and $g_{2,S} \propto t^0$ regimes. More precisely, $\tau_{d,S}$ is defined as the time at which the value of $g_{2,S}$ is 2% lower than its plateau value. The results for $\tau_{d,S}$ and the corresponding plateau values of $g_{2,S}$ are listed in Table 2. It can be seen that the longest time at which we calculate the dynamic structure factor of the long probe chains (up to $t = 6 \times 10^4\tau$) is higher than the terminal time of the matrix chains of length $N_S \leq 80$. So, the results given in Figure 2 for these binary blends have included the CR contributions from both the reptation and CLF effects of the matrix chains. Figure 5 present the $\tau_{d,S}$ data as a

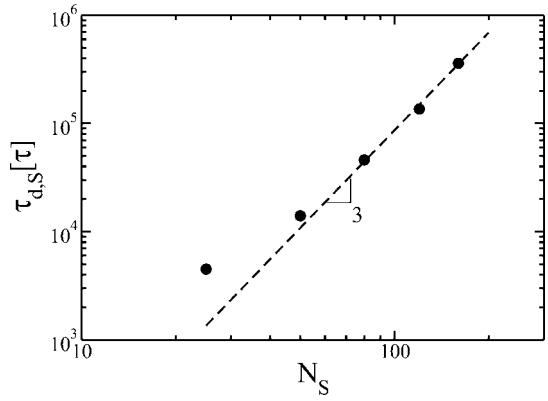

Figure 5. Terminal time $\tau_{d,S}$ of the matrix chains in binary blends as a function of their chain length N_S.

Table 3. Exponents x of the Power Law Fitting $g_{i,L}(t) \propto t^x$ to the Diffusion Curves $g_{(i = 1, 2, 3),L}(t)$ of the Long Probe Chains with Length $N_L = 350$ in Binary Blends of Various Matrix Chain Lengths N_S in the Intermediate Time Regime ($6000\tau \leq t \leq 5 \times 10^4\tau$)

N_S	$g_{1,L}$	$g_{2,L}$	$g_{3,L}$
160	0.30	0.30	0.58
120	0.32	0.31	0.61
80	0.36	0.34	0.69
50	0.42	0.39	0.76
25	0.47	0.41	0.84

function of the matrix chain length. For $N_S \geq 80$, the terminal times of the matrix chains follow a clear $\tau_{d,S} \propto N_S^3$ power law as expected from chain reptation, while the $\tau_{d,S}$ values at $N_S \leq 50$ corresponds to a crossover from the Rouse behavior of $\tau_{d,S} \propto N_S^2$ to the reptation behavior. Compared with the pure reptation prediction of $\tau_{d,S} = 3\tau_e(N_S/N_e)^3 \approx 0.74N_S^3\tau$ using $\tau_e = 2290\tau$ and $N'_e = 21$, the simulation results on $\tau_{d,S}$ ($\approx 0.087N_S^3\tau$) are smaller by a factor of about 8.5, indicating the strong contour length fluctuations and constraint release effects on the relaxation of these short matrix chains. Our simulations of the monodisperse melts of chain length $N \leq 80$ have yielded the same terminal times as that of the corresponding matrix chains $\tau_{d,S}$ in the binary blends. Thus the diluted long probe chains in binary blends have only a very weak influence on the relaxation of the matrix chains.

Note in Figure 4 that the slopes of the $g_{1(2),L}(t)$ curves of the binary blends increase with decrease of N_S in the intermediate time regime. This is consistent with the theoretical expectation from the reduced terminal relaxation time $\tau_{d,S}$. But the deviation of these diffusion curves from the pure reptation behavior of $g_{1(2)} \propto t^{1/4}$ occurs right after τ_e instead at the longer time scale of $\tau_{d,S}$. This is most evident for $N_S = 160$. There, the CR effect leads to a faster diffusion of the long probe chains in the time region $\tau_e \leq t \leq \tau_R$, even though $\tau_{d,S}$ of these matrix chains is greater than the Rouse time τ_R of the probe chains. The time dependency of the $g_{1(2),L}$ data in the intermediate regime can be described by a power law scaling of $g_{1(2),L}(t) \propto t^x$. Fitting the $g_{1(2),L}$ results in the time region of $6000\tau \leq t \leq 5 \times 10^4\tau$, the value of the exponent x is found to increase with decreasing N_S, going from $x = 0.30$ for $N_S = 160$ to 0.42(0.39) for $N_S = 50$, see Table 3. These values indicate a monomer diffusion faster than that of pure reptation (0.25) but slower than the free 3D Rouse motion (0.5) even for a matrix chain length as short as $N_S = 50$. At longer time scales, the contribution from constraint release becomes more prominent, leading to an upturn of the monomer diffusion curves, approaching the coherent Rouse motion power law of $t^{1/2}$ earlier than the Rouse time τ_R of the same chains in the monodisperse melt. This can be seen more clearly in Figure 4a, where the onset of the $g_{1,L} \propto t^{1/2}$ regime shifts to earlier times with decrease of the matrix chain length. Following the coherent Rouse motion regime, our simulation results in Figure 4 also show an upturn of the $g_{1,L}(t)$ curve toward the free diffusion $\propto t^1$ power law and equivalently a level-off of the $g_{2,L}(t)$ curve toward a plateau value of $140 \pm 15\sigma^2$, which is comparable to the mean square radius of gyration of the probe chain $R_g^2(350) \approx 185\sigma^2$. The crossover point between the $g_{1,L} \propto t^{1/2}$ and $g_{1,L} \propto t^1$ or between the $g_{2,L} \propto t^{1/2}$ and $g_{2,L} \propto t^0$ regimes also shifts to shorter times with the reduced N_S and occurs much earlier than the terminal time τ_d of the long chains expected from the monodisperse melt. A more quantitative discussion of the chain length dependence of the long chain terminal time, however, would require a simulation time longer than that performed in the current work.

In Figure 4 we have also included the $g_{1(2),L}(t)$ data obtained from the binary blend with a matrix chain length $N_S = 25$, which is about one entanglement length long ($N_e^P = 23$). The monomer diffusion of the long probe chains in this system presents the same free Rouse diffusion behavior before and after τ_e. But there is a slowdown of the diffusion at intermediate time scales ($g_{1,L} \propto t^{0.47}$, see Table 3), before a return to the $t^{1/2}$ power law. This behavior is presumably related to the nonvanishing entanglements of the probe chains with the surrounding matrix chains, even for N_S as small as 25. The occasional entanglements between two long probe chains could also retard their free Rouse diffusion, because this effectively increases the molecular weight when the two entangled probe chains move together for a certain time period. This effect is not important for the probe chains in the well-entangled matrix where the chain reptation and tube reorganization are not sensitive to the addition of one or two topological constraints with longer lifetime.

The results for the mean square monomer displacement $g_{1,L}(t)$ should be separable into two parts: a contribution from the reptation of the long probe chain itself and a contribution from the constraint release effect due to the rapid motion of the surrounding matrix chains. Since the CR effect in the monodisperse melt is rather weak, one can in principle use the simulation data on $g_1(t)$ from the monodisperse system as a reference for the reptation contribution. After subtracting this contribution from the total $g_{1,L}(t)$ results given in Figure 4a, the remaining part, $\Delta g_{1,L}(t) = g_{1,L}(t) - g_1(t)$, is plotted in Figure 6 for time scales longer than τ_e. According to the independence assumption of eq 13, $\Delta g_{1,L}(t)$ is expected to reflect the contribution from the tube Rouse motion and thus follow the scaling law of eq 11, which is sketched as the thick dashed line in Figure 3. However, Figure 6 shows some obvious discrepancies between the simulation data and the theoretical expectation in the intermediate time regime ($\tau_e \leq t \leq \tau_R$). First of all, the significant increase of $\Delta g_{1,L}(t)$ in the time region $\tau_e < t < \tau_{d,S}$ was not anticipated in the original theoretical framework which neglects the effect of contour length fluctuations of the matrix chains on constraint release.[18] Second eq 11 predicts a power law dependence of $\Delta g_{1,L} \approx g_{1,L}^{tube} \propto t^{1/2}$ for $\tau_{d,S} \leq t \leq \tau_{R,L}^{Rouse}$ starting from $g_{1,L}^{tube}(\tau_{d,S}) \approx d_T^2$. But the slopes of the $\Delta g_{1,L}(t)$ curves (≥ 0.65) in Figure 6 are higher than 1/2 for almost the entire intermediate time regime. The actual values of $\Delta g_{1,L}(\tau_{d,S})$ at the time $\tau_{d,S}$ obtained from different binary blends are around $10\sigma^2$, which is smaller than the predicted $g_{1,L}^{tube}(\tau_{d,S})$ value of about $70\sigma^2$ using the tube diameters estimated by primitive path analysis ($d_T^P = 8.6\sigma$)[10] and other other analysis algorithms ($d_T \approx 8 \sim 10\sigma$). These discrepancies could be attributed to the use of a single mean waiting time τ_{obs} or $\tau_{d,S}$ for constraint release in the theoretical treatments.[14]

The theoretically expected $\Delta g_{1,L} \propto t^{1/2}$ power law is achieved at larger time scales close to and beyond the Rouse time $\tau_{R,L}$ of the probe chains. The fitting curves of $\Delta g_{1,L} = A(t/\tau)^{1/2}$ in the long time region are shown as solid lines in Figure 6 and have

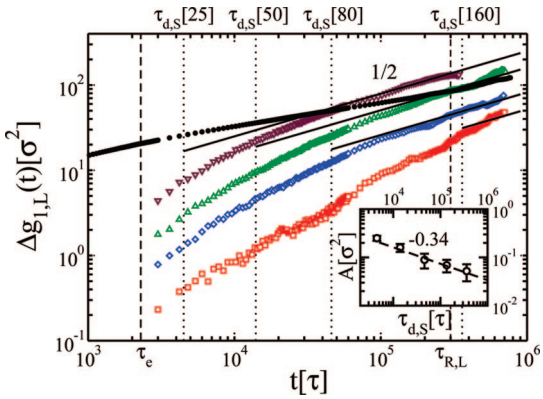

Figure 6. Difference, $\Delta g_{1,L}$, between the $g_{1,L}$ values of the long probe chains of length $N_L = 350$ in binary blends and that of the chains with the same length in the monodisperse melt as a function of time, calculated from the simulation data of $g_{1,L}$ in Figure 4. The symbols correspond to the binary blends with different matrix chain lengths: $N_S = 160$ (square), 80 (diamond), 50 (triangle-up), and 25 (triangle-down). The filled circles are the simulation results of $g_1(t)$ obtained in the monodisperse case. The dotted vertical lines represent the terminal times $\tau_{d,S}$ of the short matrix chains as given in Table 2. The dashed vertical lines represent the equilibration time τ_e and Rouse time $\tau_{R,L}$ of the probe chains, respectively. The solid lines show the power law fitting of the simulation data to $\Delta g_{1,L} = A(t/\tau)^{1/2}$ at large time scales and have been extrapolated down to the terminal time of the matrix chains. The values of the fitting parameter A are given in the inset as a function of $\tau_{d,S}$.

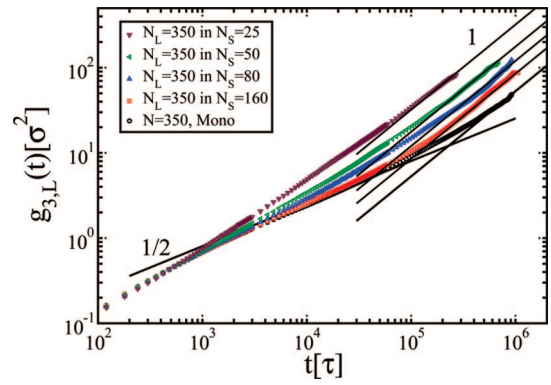

Figure 7. Mean square displacement $g_{3,L}(t)$ of the center of mass of the long probe chains with 350 monomers in binary blends with various short matrix chains.

been extrapolated down to the terminal times of the short matrix chains $\tau_{d,S}$ for different binary blends. Supposing a constant tube diameter d_T, eq 11 predicts that the value of the parameter A should be proportional to $\tau_{d,S}^{-1/2}$ as $A \approx d_T^2/(\tau_{d,S}/\tau)^{1/2}$. The fitting results on A are presented in the inset of Figure 6. These data points, however, exhibit a weaker power-law dependence on $\tau_{d,S}$ (or N_S) than the $\tau_{d,S}^{-1/2}$ (or equivalently $N_S^{-3/2}$) tube Rouse behavior, yielding $A \propto \tau_{d,S}^{-0.34\pm0.03}$ ($A \propto N_S^{-0.94\pm0.05}$) for $N_S \geq 50$. The scaling of $\Delta g_{1,L} \propto t$ expected for $t \geq \tau_{R,L}^{tube}$ is not clearly observed in Figure 6, indicating that the tube Rouse time $\tau_{R,L}^{tube}$ (eq 12) has not been reached by our simulations. In addition, Figure 6 demonstrates that the tube Rouse contribution, $\Delta g_{1,L}$ ($g_{1,L}^{tube}$), dominates over the reptation contribution, $g_{1,L}^{rep}$, only for the binary blends with very short matrix chains $N_S \leq 50$. Since the dynamics of the long chains is already Rouse-like in the matrix of chain length $N_S = 25$, there is a very limited parameter space left for the tube Rouse dominant regime of the semiflexible probe chains with $N_L = 350$ monomers. The weak N_S dependence of the long-chain diffusion and the corresponding narrow window of the CR Rouse dominant regime will be discussed in more detail in section 3.2.2.

The above comparison between the theoretical predictions and the simulation results may also be affected by some other factors. Since the length of some of the matrix chains we studied are rather short ($N_S \leq 80$) relative to the entanglement length ($N_e^p = 23$), contour length fluctuations will affect the relaxation of the whole matrix chain, while in theoretical models the matrix chain length is usually assumed to be sufficiently long so that the CLFs only affect the ends of the chains. The use of the $g_1(t)$ data of the monodisperse melt as a reference for the pure reptation contribution is also an approximation, especially at longer time scales. Experimental measurements of the viscoelastic properties of monodisperse polymer melts have shown that constraint release effects are non-negligible even for monodisperse chains of entanglement densities as large as $Z = 30$.[24,56] The neglect of CR effect in the monodisperse case could affect the quantitative interpretation of Figure 6. In addition, the experiments of Watanabe et al. have suggested that the independence of tube Rouse motion and chain reptation is an inadequate assumption for binary blends with diluted long probe chains.[24] The relaxation rate of the actual CR process depends on the configuration of the probe chain, and the contour length of its confining tube may not be preserved during the local CR jumps.[24,57] These features are not considered in the standard CR Rouse model.[17,18,28] The higher slopes of the $\Delta g_{1,L}(t)$ curves in the intermediate time regime than the theoretical prediction based on a fixed tube diameter[18] could be understood by an effective tube dilation progressing with time in this region.[11] The tube dilation mechanism is thought to be important for binary blends with Struglinski−Graessley parameter $r_{SG} \geq 0.064$,[19] and most of the binary systems we simulated satisfy this condition; see Table 1. Doi et al. have proposed a theoretical framework for considering the tube dilation process[17] which might be used to interpret our simulation results, supposing that the distribution of the topological constraint lifetimes is incorporated into their theory.

3.2.2. Chain Diffusion. The pure reptation model predicts the mean square displacement of the center of mass $\mathbf{R}$ of an entangled chain, $g_3(t) = \langle(\mathbf{R}(t) - \mathbf{R}(0))^2\rangle$, as[2,9]

$$g_3^{rep}(t) = \begin{cases} 6\dfrac{b^2}{N}Wt, & t \lesssim \tau_e \\ \dfrac{d_T^2}{N}(Wt)^{1/2}, & \tau_e \lesssim t \lesssim \tau_R \\ 2\dfrac{d_T^2}{N^2}Wt, & \tau_R \lesssim t \end{cases} \quad (14)$$

The crossover from the $g_3 \propto t^{1/2}$ to $g_3 \propto t$ power laws around τ_R is captured by our simulations results for the $g_3(t)$ curve of the monodisperse melt with $N = 350$ in Figure 7.

Equation 14 predicts that at long time scales ($t > \tau_R$) the diffusion of the whole polymer chain follows the scaling law of $g_3(t) \approx D^{rep}t$ with the diffusion coefficient $D^{rep} \propto N^{-2}$. In Figure 8 we plot the diffusion coefficient D_S of the short matrix chains obtained by fitting their $g_{3,S}(t)$ curves in the terminal regime to the relation of $g_{3,S}(t) = 6D_St$ for the binary blends with same short chain segment fraction $n_S = 0.85$. For comparison, the self-diffusion coefficients of certain short chains in their corresponding monodisperse melts are also presented. The D_S values of the matrix chains are found to be slightly (less than 11%) smaller than their self-diffusion counterparts, reflecting the weak perturbations imposed by the diluted long probe chains on the diffusion of these short chains. This difference increases with increasing N_S owing to the enhanced entanglements between the long and short chains. For instance, the diffusion coefficient of the matrix chains of length $N_S = 50$ is about 3% smaller than that in their monodisperse case, while this relative difference is about 11% for the $N_S = 80$ chains.

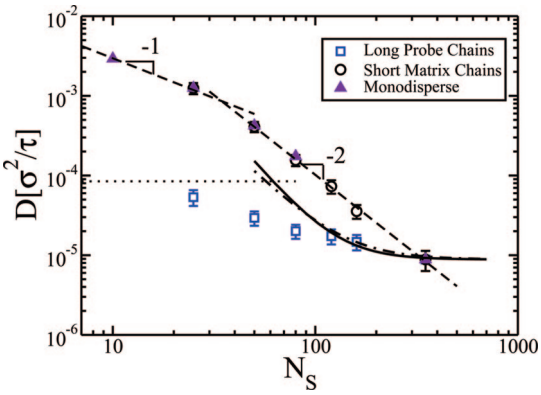

Figure 8. Diffusion coefficients of the long probe chains, D_L, with length $N_L = 350$ and the short matrix chains, D_S, as a function of the matrix chain length N_S in binary blends with fixed long chain segment fractions $n_L = 0.15$. The triangles are simulation results obtained from monodisperse melts with fixed chain segment number density $\rho = 0.85\sigma^{-3}$. The thick solid and dotted-dashed lines are the predictions of eqs 15 and 16, respectively, using the z and K values from the experimental work of Green et al.[21] The dotted horizontal line shows the Rouse diffusivity of the probe chains, D_L^{Rouse}, attained in the matrix offering only frictional, and not topological, resistence to the long chain motion.

The simulation results on D_S demonstrate a clear crossover from the Rouse diffusion of $D_S \propto N_S^{-1.0 \pm 0.1}$ to the $N_S^{-2.0 \pm 0.2}$ dependence expected by reptation. A similar crossover behavior has been observed by Kremer et al. in their MD simulations of monodisperse flexible polymer melts.[8] In experimental studies of the self-diffusion coefficient D_{self}, since both the glass transition temperature and the thermal expansion coefficient of free volume are functions of the molecular weight in the unentanglement region, it is essential to correct the results to a constant free volume state (or constant monomeric frictional coefficient state) in order to observe the Rouse to entanglement regimes transition.[21,24,33] Otherwise, the diffusion coefficient might show a single power law $D_{self} \propto N^{-2}$ for the entire range of chain length.[33] The use of a canonical ensemble at constant volume in our MD simulations can minimize this problem. The simulated diffusion coefficients of the short chains can be described by a scaling law of $D_S^{Rouse} \approx 0.03N_S^{-1}\sigma^2/\tau$ in the Rouse regime, where $N_S \leq 25$, and of $D_S \approx 1.02N_S^{-2}\sigma^2/\tau$ in the entanglement region, where $N_S \geq 50$.

Since the matrix chains studied in Figure 8 are still relatively short, the N_S^{-2} dependence of D_S should not be understood as a direct result of pure reptation. It is rather a collective effect of reptation, CLF and CR dynamic modes. According to the pure reptation model, the chain diffusion coefficient in the reptation regime is $D_S^{rep} = D_S^{Rouse}/3Z_S$ with $Z_S = N_S/N_e$.[2] If the simulation results on the $D_S(N_S)$ scaling laws in the Rouse and entanglement regimes are directly substituted into this expression, the resulted entanglement length is $N_e \approx 102$, which is much too large in comparison with the primitive path analysis result of $N_e^P = 23$.[10] The higher chain diffusivity observed in simulations than the pure reptation prediction indicates the strong effect of contour length fluctuations and constraint release over the range of chain lengths studied in the current work. It also illustrates that the agreement of the exponent (−2) with the value for pure reptation by itself does not guarantee that a pure reptation regime has actually been achieved. Experimentally, the self-diffusion coefficient exhibits a crossover behavior in which the exponent ν in $D_{self} \propto N^{\nu}$ changes from $\nu > 2.0$ ($\nu \approx 2.3 \sim 2.5$) when N is slightly larger than N_e and converges to the asymptotic limit of $D_{self} \propto N^{-2}$ when N/N_e is larger than 10−20.[30] If the CR effects are suppressed by diluting a low concentration of tracer chains into a matrix of sufficiently long chains, then the tracer diffusion coefficient follows the scaling law of $D_{tr} \propto N^{-2}$ over the entire entanglement region.[21,30]

The $g_{3,L}(t)$ curves of the probe chains of length $N_L = 350$ in various binary blends are presented in Figure 7. Below the entanglement time τ_e, all the $g_{3,L}(t)$ curves coincide with each other, giving a scaling of $g_{3,L} \propto t^{0.70}$. Above τ_e the diffusion of the long probe chains is accelerated by the CR events caused by rapid motion of the short matrix chains. The slopes of the $g_{3,L}$ curves increase with decrease of N_S in the intermediate time regime. Similar to the $g_{1(2),L}$ curves, the time dependence of $g_{3,L}$ in this region could also be described by a power law relation $g_{3,L} \propto t^x$. The fitting results of the exponent x are given in Table 3, which shows an increase of the x value from 0.58 to 0.84 when N_S is reduced from 160 to 25. In the MD simulations of Barsky for binary blends of linear flexible polymer chains, a similar power law fitting to the $g_{3,L}(t)$ curves of the probe chains with $N_L = 90$ provided an exponent x in the range of 0.83 to 0.94 for matrix chain length between $N_S = 10$ and 60.[42] The higher values of x he obtained relative to our values indicate the marginal entanglement effects in his systems. At large time scales, all $g_{3,L}(t)$ curves in Figure 7 reach the Rouse-like diffusion regime of $g_{3,L} \propto t$. The diffusion coefficients of the long probe chains are estimated by a power law fitting of $g_{3,L} = 6D_L t$ to the simulation data in this regime; see Figure 7. The resulting D_L values are shown in Figure 8, where the error bars of the data points reflect the uncertainty of the fitting. The values of D_L increase with decrease in matrix chain length. The coarse grained simulations of Picu and Rakshit on binary blends have observed a similar variation tendency of D_L with N_S in a narrower range of Struglinski−Graessley parameters.[47]

Assuming independence of the tube reorganization and chain reptation processes, the diffusion coefficient of the diluted long probe chains in a binary blend is predicted to be the linear addition of the contributions from the chain reptation $D_L^{rep} \propto R_L^2/\tau_{d,L} \propto N_L^{-2}$ and the tube Rouse motion $D_L^{tube} \propto R_L^2/\tau_{R,L}^{tube} \propto N_e^2 N_L^{-1} N_S^{-3}$ where R_L is the end-to-end distance of the probe chain.[1,18,28] Graessley has proposed an expression for the probe chain diffusion coefficient as[1,21]

$$D_L = D_L^{rep}(1 + \alpha_{cr} N_e^2 N_L N_S^{-3}) = D_L^{rep}(1 + \alpha_{cr} r_{GS}) \qquad (15)$$

where $\alpha_{cr} = (48/25)z(12\pi^2)^{z-1}$ and z is defined as the number of independent constraints per entanglement length. A somewhat different approach was suggested by Klein:[21,58]

$$D_L = D_L^{rep}(1 + KN_e^{3/2} N_L N_S^{-5/2}) \qquad (16)$$

where K is an unspecified numerical prefactor. Equation 16 is based on the conjecture that one matrix chain may be involved in multiple constraints with a long probe chain. These multiple constraints vanish simultaneously when a single matrix chain diffuses away, resulting in an enhancement of the relaxation rate in eq 16 relative to eq 15 by a factor of $(N_S/N_e)^{1/2}$. The tracer diffusion coefficients measured by Green et al. in binary blends of linear polystyrene (PS) chains agree with both predictions within the experimental precision.[21] The values of the fitting parameters were given to be $z = 3.5$ ($\alpha_{cr} = 10.95$) and $K = 5.45$, respectively.[21]

Since the asymptotic value of the reptation contribution D_L^{rep} for chains with $N_L = 350$ is not available, we use the self-diffusion coefficient of these chains in the monodisperse case as an empirical reference for D_L^{rep}. This is a somewhat crude, but still acceptable, approximation, considering that there are more than 15 entanglements per probe chain.[21,24,30] The predictions of eqs 15 and 16 using the experimental values of z and K[21] and the entanglement length $N_e^P = 23$ are plotted in Figure 8 as the thick solid and dotted-dashed curves, respectively. The tracer diffusion coefficients measured by Green et

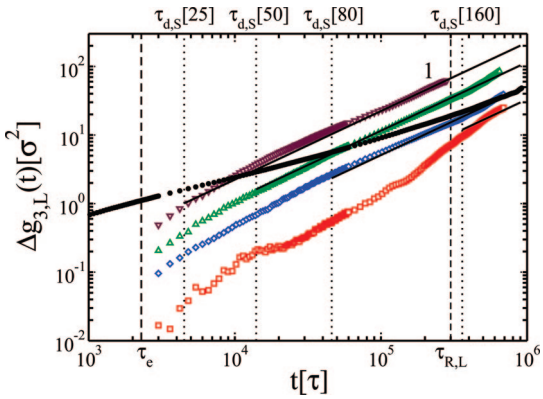

Figure 9. Difference, $\Delta g_{3,L}$, between the $g_{3,L}$ values of the long probe chains in binary blends and that of the chains with the same length in the monodisperse melt as a function of time, calculated from the simulation data of $g_{3,L}$ in Figure 7. The notations for the symbols and the vertical dotted and dashed lines are the same as that in Figure 6. The solid lines show the power law fitting of the simulation data to $\Delta g_{3,L} \propto (t/\tau)$ at large time scales and have been extrapolated down to the terminal time of the matrix chains.

al. were found to follow the predictions of eqs 15 and 16 down to the matrix chain length $N_S \approx N_c$, where N_c is the critical chain length marking the onset of the entanglements and is usually taken to be $N_c = 2N_e$.[21] The simulation results on D_L, however, show a weaker N_S dependence than in those experiments. Direct fit of the simulation data of $D_S(N_S)$ to eqs 15 and 16 in the region of $N_S \geq 50$ results in much smaller α_{cr} ($\approx$1.73 or $z \approx 0.98$) and K ($\approx$1.18) values and the fit to the data points is not satisfactory. A very similar weak dependence of D_L on N_S has been observed by Smith et al. in the tracer diffusion experiments performed on binary blends of linear poly(propylene oxide) (PPO) polymers.[31,32] In that work, the longest labeled chain had about 10 entanglements and its diffusion coefficient scaled with the shorter matrix chain length as $D_L \propto N_S^{-0.93}$ in the entanglement regime.

To understand the weak N_S dependence of D_L in our simulations, we have examined the relative contributions from constraint release effect and from chain reptation to the diffusion of the probe chains. Similar to Figure 6, the difference between the mean square displacements of the centers of mass of the probe chains in binary blends [$g_{3,L}(t)$] and in their corresponding monodisperse melt [$g_3(t)$], $\Delta g_{3,L}(t) = g_{3,L}(t) - g_3(t)$, is plotted in Figure 9 as a function of time for $t > \tau_e$. These $\Delta g_{3,L}(t)$ curves are found to follow the Rouse-like diffusion power law of $\Delta g_{3,L} \propto t^1$ for almost the entire time region above the terminal time of the short matrix chains $\tau_{d,S}$. This is expected by the tube Rouse motion model[18] and reflects that the time dependence of the CR-induced contribution to the whole chain diffusion is less sensitive to the relaxation rate distribution of the topological constraints than is that of the individual monomers (Figure 6). The results in Figure 9 show that only when the matrix chain length $N_S \leq 80$, does $\Delta g_{3,L}(t)$ start to dominate over the reptation contribution $g_3(t)$ (filled circles) at large time scales, consistent with the results of $\Delta g_{1,L}(t)$ shown in Figure 6. This means that the CR Rouse dominant regime, where $D_L \propto N_S^{-3(2.5)}$, for the probe chains of length $N_L = 350$ can only exist in the region of matrix chain length $N_S < 80$. On the other hand, the critical chain length is $N_c \approx 2N_e^p = 46$ in the melts of semiflexible chains. When N_S is reduced to 25, the dynamics of the probe chains already enters the Rouse regime as reflected by the Rouse-like behavior of their $g_{1,L}(t)$ and $g_{3,L}(t)$ curves. In this case, the value of the diffusion coefficient D_L ($\approx 5.35 \times 10^{-5}\sigma^2\tau^{-1}$) is quite close to the Rouse diffusivity of these probe chains, D_L^{Rouse}, attained in the matrix offering only frictional, and not topological, resistence to the long chain motion. The D_L^{Rouse} value is estimated to be $^{-}D_L^{Rouse} = k_BT/N_L\zeta^R \approx 8.46 \times 10^{-5}\sigma^2\tau^{-1}$ (dotted horizontal line in Figure 8) by using the effective monomer friction coefficient $\zeta^R = k_BT/N_SD_S^{Rouse} \approx 33.8k_BT\tau\sigma^{-2}$ obtained in the Rouse regime. The window measured in N_S ($N_c < N_S < 80$) for the CR Rouse dominant regime is thus too narrow to be observed for the semiflexible probe chains of length $N_L = 350$ or 15.2 entanglements. The slow increase of the simulation D_L data with decreasing N_S in fact corresponds to a crossover from the CR Rouse dominant regime to the Rouse regime in the binary blends of semiflexible chains. Fitting the $\Delta g_{3,L}(t)$ curves in Figure 9 to $\Delta g_{3,L} = 6D_L^{CR}t$ in their linear region yields the N_S dependence of the CR contribution to the diffusion coefficient as $D_L^{CR} \propto N_S^{-1.03}$ for $N_S \geq 50$, much weaker than the $D_L^{Tube} \propto N_S^{-3(2.5)}$ scaling of pure tube Rouse behavior. The total range of the D_L value accessible to the probe chains is defined by its upper and lower bound values, D_L^{Rouse} and D_L^{rep} ($\approx 8.84 \times 10^{-6}\sigma^2\tau^{-1}$), and covers only about one decade. In contrast, the diffusion coefficient of the PS tracer chain with similar number of entanglements ($Z = 14.2$ for $M = 255$ kg/mol and $M_e = 18$ kg/mol) used by Green et al. has been shown to vary by more than two decades with the decrease of the matrix chain length.[21] In Figure 8 the prediction curves obtained by using the experimental z and K values reach the upper bound of D_L^{Rouse} at $N_S \approx 58$, where the matrix chains are still entangled, leaving no space for the Rouse diffusion regime of the probe chains; thus they overestimate the D_L values in the region of low matrix chain length.

The difference in long-chain diffusion behavior observed in simulation vs experimental studies of binary blends with comparable number of entanglements, Z_L, per probe chain indicates that the dynamics in binary blends is not determined only by the number of entanglements per chain, but also by other molecular factors, such as the chain stiffness and the chain-length-dependence of the monomer friction coefficient which can be significant in real melts. In polymer melts, the stiffer chains possess a smaller packing length p, and correspondingly a smaller entanglement length N_e by a power law $N_e \propto p^3$.[59] Experimentally, the value of the entanglement length N_e or the critical chain length N_c has turned out to be another factor affecting the tracer diffusion coefficient D_L in addition to Z_L. For instance D_L of the PPO polymers with critical molecular weight $M_c = 7$ kg/mol shows a much weaker matrix chain length dependence than that of the PS polymers with $M_c = 35$ kg/mol.[21,32] On the other hand, in binary blends of polybutadienes with even smaller M_c value (3.8 kg/mol), the CR contribution to the tracer diffusion coefficient, reflected by the values of parameters z and K in eqs 15 and 16, is found to be stronger than in PS/PS blends.[60] A recent experimental examination of the linear viscoelastic behavior has also shown that the CR-dominance is more easily achieved in binary blends of linear polyisoprenes ($M_e = 5$ kg/mol) than in the PS/PS blends.[61] It was thus suggested that in addition to the number of entanglements per chain and the relaxation time within the segment, the entanglement dynamics could also be affected by other factors such as the effective topological constraints per entanglement segment (z in eq 15) that is related to the packing length.[61] In the melts of bead-spring model chains studied in MD simulations, the packing length and entanglement length are $p = 0.36$ and $N_e^p = 23$ for the semiflexible chains with $k_\theta = 2$ in eq 3 and $p = 0.68$ and $N_e^p = 65$ for flexible chains with $k_\theta = 0$, respectively.[10] The effective monomer friction coefficients ζ in these two types of melts are also found to be different. By use of the relation of $\zeta^e = k_BT/Wb^2$ for monodisperse melts of linear entangled polymers, ζ^e is estimated to be about $25.0k_BT\tau\sigma^{-2}$ for the flexible chains[8,9] and about $50.0k_BT\tau\sigma^{-2}$ for the semiflexible chains used in the current work. These ζ^e values determined from the long entangled polymer melts are

higher than that calculated from melts of short unentangled chains, as known from diffusion and viscoelasticity experiments.[8] The values of ζ estimated from the short chains, using the Rouse diffusion relation of $\zeta^R = k_BT/N_SD_S^{Rouse}$, are $\zeta^R \approx 16k_BT\tau\sigma^{-2}$ for the flexible chains[8] and $\zeta^R \approx 33.8k_BT\tau\sigma^{-2}$ for the semiflexible chains, respectively. In both entangled and unentangled regimes, the monomer friction coefficient of the semiflexible chains is about twice as large as that of the flexible chains. Likhtman et al. have also pointed out that the dependence of the plateau modulus G_N^0 on the packing length p follows different scaling laws in the semiflexible and flexible polymer melts.[62] It would be interesting to perform systematic simulations to investigate the relation between the dynamics in binary blends and the polymer chain stiffness.

Since our binary blends are not in the dilute limit for the long probe chains, the diffusion of these probe chains could possibly be slowed down by mutual entanglements among themselves. But this effect should still be rather weak for the systems with $N_L = 350$ and $n_L = 0.15$. This can be seen from the attainment of Rouse-like behavior of the probe chains in the matrix with $N_S = 25$ and the very similar D_L values obtained from the binary systems with same long and short chain lengths ($N_L = 350$ and $N_S = 80$) but different long chain segment fractions, $n_L = 0.15$ and $n_L = 0.20$, respectively. It should also be noted that our simulation results for $g_{3,L}(t)$ still have some fluctuations in the long time regime due to limited MD simulation time, which is still below the terminal relaxation time $\tau_{d,L}$ of the long probe chains. This might also affect the precision of the simulation results on the diffusion coefficients. Larger scale simulations with longer probe chains and lower probe chain concentrations are still needed to give better comparison with experiments.

3.3. Packing and Diffusing of Matrix Chains in the Tube Region of the Probe Chains. Since MD simulations yield the three-dimensional coordinates of each individual monomer as a function of time, one could in principle get a microscopic picture of the constraint release events by monitoring the diffusion of the matrix chains in the neighboring region of a probe chain. However, since the probe chain itself is relaxing on all length and time scales and the confining tube is a conceptual entity, to distinguish the effect of the motion of one individual matrix chain on the relaxation of the probe chain is very difficult, if not impossible. Nevertheless, in this section, we present a preliminary analysis of the packing and diffusing behavior of the matrix chain segments in the tube-like region of the long probe chains in order to provide some microscopic pictures which could be related to the constraint release effect.

First, we need to define a tube region for the probe chain. This relies on the identification of the primitive path which is the centerline of the confining tube. Since we are interested in the CR-related relaxation of the chains, the length or quadratic energy minimization methods used in the primitive path identification,[10,11,63] which freeze the chain ends and consequently suppress the constraint release, are not directly applicable for this purpose. As an alternative, we employ the concept of primitive chain first suggested by Kremer et al. for visualizing chain reptation.[8] The primitive chain of a long probe polymer is constructed in a continuous coarse-graining manner by subdividing the probe chain into $N_p = (N_L + 1 - N_e)/2$ subunits with the position $\mathbf{R}_i^p$ of subunit or monomer i of the primitive chain given by

$$\mathbf{R}_i^p = \frac{1}{N_e}\sum_{j=2i-1}^{2(i-1)+N_e} \mathbf{r}_j \qquad (17)$$

Here $\mathbf{r}_j$ is the coordinate of monomer j of the real probe polymer. The motion of the primitive chain is much more confined and essentially has to follow the center of the confining tube.[8] The tube region of a test polymer chain is then defined as the space that is within one-half of the tube diameter $d_T = N_e^{1/2}b$ from the monomers of the corresponding primitive chain. In the following analysis, we exclude the first 35 monomers on each end of the primitive chain from the definition of the tube region in order to avoid the effects of the fast moving chain ends. In other words, for a probe polymer chain of length $N_L = 350$, only the central 94 monomers out of the total $N_p = 164$ monomers of its primitive chain are considered in the calculations related to the tube region. For the results presented below, the value of $N_e^p = 23$ is employed to define the size of the entanglement segments and the diameter of the tube d_T. The use of other reasonable values for the entanglement length N_e only affects the quantitative results without causing any qualitative changes in the physical picture.

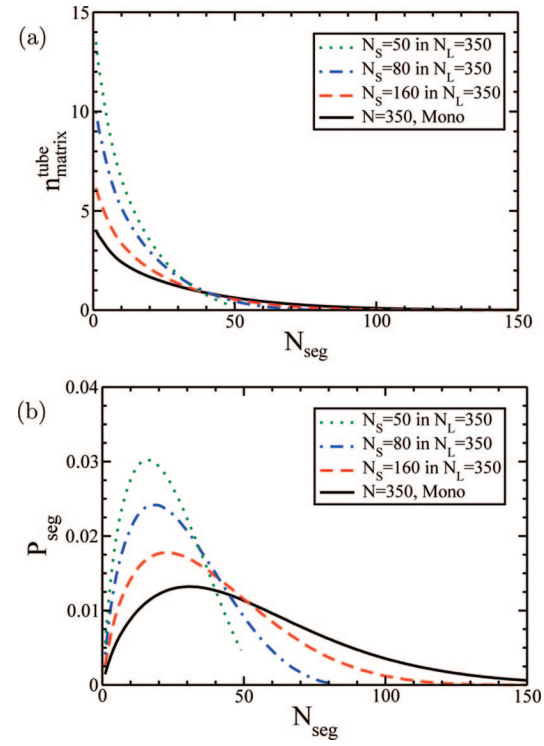

Figure 10. (a) Average number of short matrix chains, n_{matrix}^{tube}, which have a number of N_{seg} monomers inside the tube region of a long probe chain as a function of N_{seg}. (b) Probability of finding a matrix chain monomer, P_{seg}, inside the tube region of a long probe chain, belonging to a matrix chain which has N_{seg} monomers inside the same tube. In all the binary blends, the long probe chains have a fixed chain length of $N_L = 350$ and monomer number fraction of $n_L = 0.15$. The calculations are restricted to the tube region defined by the central 94 monomers of the primitive chain of the long probe polymer.

As per the above definition of the tube, all the monomers of the matrix chains, which have a center-to-center distance $\leq d_T^p/2$ from any of the central 94 monomers of the primitive chain of a probe polymer, are considered to be located inside the tube region of that probe polymer. Since the global number density of chain segments is fixed ($\rho = 0.85\sigma^{-3}$), the average number of monomers inside the studied tube region of each probe chain is also nearly the same (2800 ± 80) in all melt systems with $N_L = 350$. For binary blends with $n_L \approx 0.15$, there are $N_{tot}^{tube} = 2400 \pm 50$ monomers from the matrix chains and the rest are from other probe chains. In Figure 10a, we present the analysis results on the average number of matrix chains, n_{matrix}^{tube}, which have a nonzero number of monomers N_{seg} inside the tube region, as a function of N_{seg}. Correspondingly, Figure 10b gives the probability P_{seg} for a matrix chain monomer that is located in the tube region of a probe chain to belong to a matrix chain

which has N_{seg} monomers inside the same tube, i.e., $P_{seg}(N_{seg}) = N_{seg} n^{tube}_{matrix}(N_{seg})/N^{tube}_{tot}$. The peaks in Figure 10b represent the most probable segment length of a matrix chain involved in the confinement or entanglement of the long probe chain. This peak is located at $N_{seg} = 31$ in the monodisperse case and shifts to lower N_{seg} values with decreasing N_S, due to the higher concentration of the matrix chain ends in the tube region. Figure 10b also reveals that for the binary blend with $N_S = 160$ more than 33% of the monomers inside the tube belong to matrix chain segments with $N_{seg} \geq 2N_e^P$. These matrix chain segments span several entanglement volumes, and their diffusion out of the tube region could possibly lead to multiple constraint release events, as conjectured by Klein.[58] The relatively high probability of finding the matrix chain segments with $N_{seg} \geq 2N_e^P$ inside the confining tube might result from the semiflexible character of the bead-spring model chains we used in the current work.

Since the microscopic description of the topological constraints or entanglements between chains is still not clear,[8,64] a measurement of the lifetimes of the topological constraints that the surrounding matrix chains impose on a certain long probe chain is not straightforward. In this work, we compute the probability distribution of the lifetimes t_{life} over which the short matrix chains stay inside the tube region of the probe chains, which should be closely related to the distribution of the waiting times of constraint release events. As shown in Figure 10a, there are a substantial number of matrix chains which have only a few monomers in the tube region of the probe chains. These chains can diffuse in and out of the tube very quickly. To avoid the large noise caused by the rapid chain motions, we limit our analysis to the matrix chains that have a significant number of monomers ($N_{seg} \geq N_e^P/2$) in the tube region and thus are likely to effectively contribute to the entanglements with the corresponding probe chain.[64] The lifetime t_{life} is defined as follows. When a matrix chain first has $N_{seg} = N_e^P$ monomers inside the tube region of one probe chain, we switch on a time counter for this pair of matrix and probe chains. The value of N_{seg} changes with time due to the reptation and fluctuations of the matrix chain. When a large enough part of the matrix chain has diffused away that only $N_{seg} = N_e^P/2$ monomers are left in the tube region, we switch off the time counter. The time interval between the on and off points of the time counter is taken to be t_{life} for this interaction between the probe and matrix chains. The same procedure is repeated for all pairs of matrix and probe chains over the whole time period analyzed. In our MD simulations the configurations of the chains are saved after each time interval of 60τ. The analyses are carried out in the time period starting from the simulation time $t = 6.9 \times 10^4\tau$ to the end of the simulation run. The total number of interactions, $N_{life}(t_{life})$, are collected into bins with a bin width of 300τ. For a direct comparison between the different binary blends, the results for $N_{life}(t_{life})$ are normalized by the total number of long probe chains in each system and also by the total analysis time duration. The exact values of N_{seg} chosen for the on (N_e^P) and off ($N_e^P/2$) criteria for the time counter have only quantitative effects on the analysis.

Figure 11 presents the normalized results for $N_{life}(t_{life})$ for different binary blends. This figure clearly demonstrates the broad probability distribution of lifetimes of the interactions, ranging from time scales of the order of τ_e to above the terminal time $\tau_{d,S}$ of the matrix chains. For time scales shorter than $\tau_{d,S}$, N_{life} shows a quasi-power-law dependence on t_{life} as $N_{life} \propto t_{life}^{-2}$, but it drops quickly after $\tau_{d,S}$. The latter phenomenon is more evident for the binary blends with shorter matrix chains due to the limited MD simulation time. Since the probability is such a steeply decreasing function of t_{life}, the mean lifetime of these interactions is significantly smaller than the terminal time $\tau_{d,S}$ of the matrix chains. The broad distribution of $N_{life}(t_{life})$ indicates

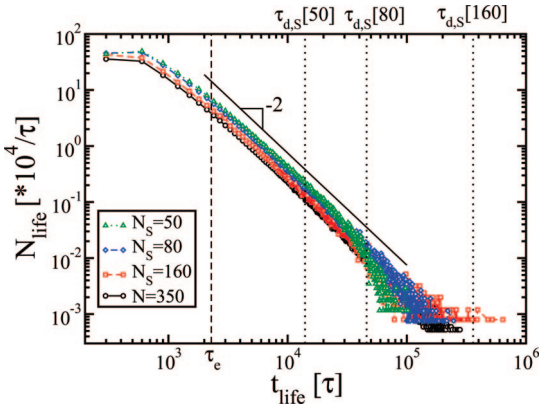

Figure 11. Average number of events N_{life} in which the matrix chains stay inside the tube region of a long probe chain for a lifetime t_{life}. The results have been normalized by the total time duration of the analysis. The parameters for the long probe chains are the same as that in Figure 10. The dotted vertical lines represent the terminal times $\tau_{d,S}$ of the short matrix chains as given in Table 2, and the dashed vertical line represents the entanglement time τ_e.

the importance of a thorough consideration of the relaxation rates of the topological constraints in order to obtain a good description of the dynamic properties of polymer melts at all time scales or frequencies.[3,14,15] It is also noteworthy in Figure 11 that the difference between the $N_{life}(t_{life})$ data obtained from binary blends with various matrix chain lengths is not as large as that expected from constraint release theory, which suggests that the mean constraint lifetime should be proportional to the matrix chain terminal time. The broad distribution of lifetimes reflects that the matrix chains are not always penetrating deeply or orthogonally into the tube region of the long probe chains, and thus often do not need to diffuse their entire contour length through the tube to release the constraint. As a final remark, since the matrix chains are moving in and out of the tube regions continuously at all time scales, a true constraint release event is likely a collective effect of all the matrix chain segments in the same entanglement volume. The assumption frequently used in models (such as slip-link models) that the departure of one matrix chain could induce a topological constraint release event is thus seen to be a very much oversimplified approximation. This could partly explain the difference between the distribution of $N_{life}(t_{life})$ given in Figure 11 and the probability distribution function proposed by Rubinstein et al. based on the single chain relaxation function (see section 3.4), which defines a higher probability at time scales closer to the terminal time of the short chains.[14]

3.4. Coarse-Grained Tube Fluctuation Model. In this section, we provide a further examination of the ability of the constraint release Rouse motion model to predict the relaxation dynamics of binary blends. To do so, we incorporate the tube Rouse motion model into the coarse-grained simulation algorithm recently proposed by Zhou and Larson for studying the dynamics of entangled linear polymers and asymmetric polymer stars.[39] In that simulation, the curvilinear Rouse motion of an entangled linear polymer along a confining tube is represented by the diffusion of a one-dimensional (1D) Rouse chain along a three-dimensional random walk with the step size equal to the tube diameter. The governing equations for a 1D Rouse chain with N_R springs are given as[2,39]

$$\zeta_R \frac{dR_i}{dt} = -K_R(2R_i + R_{i+1} + R_{i-1}) + f_i, \quad \text{for } i = 2, ..., N_R - 1 \tag{18}$$

$$\zeta_R \frac{dR_0}{dt} = -K_R(R_0 - R_1) + f_0 - \frac{3k_BT}{d_T}, \quad \text{for } i = 0 \tag{19}$$

$$\zeta_R \frac{dR_{N_R}}{dt} = -K_R(R_{N_R} - R_{N_R-1}) + f_{N_R} + \frac{3k_BT}{d_T}, \quad \text{for } i = N_R \tag{20}$$

where R_i is the 1D coordinate of Rouse bead i, K_R is the spring constant, ζ_R is the drag coefficient, and f_i is the Gaussian random force which follows $\langle f_i(t)\rangle = 0$ and $\langle f_i(t)f_j(t')\rangle = 6k_BT\delta_{ij}\delta(t - t')$. The curvilinear length of the 3D random walk representing the confining tube is set to be just long enough to contain the Rouse chain. Since the tube and the Rouse chain share the same one-dimensional path, the 1D positions of the Rouse beads can be directly mapped onto their corresponding 3D coordinates along the tube. The 3D Rouse bead coordinates are then used for analyzing the dynamic relaxation of the represented entangled linear polymers. In the original work of Zhou and Larson, the tube contour was fixed in space, except at the ends where random-walk steps or tube segments were added to contain any part of the Rouse chain that diffused out of the previously existing tube, while the tube segments were deleted when they were evacuated by the chain. The tube segments still occupied by the Rouse beads remain in place.

To introduce the tube Rouse motion mechanism into the above coarse-grained (CG) simulation model, we refer to the assumptions of Graessley that the local jump of the tube contour occurs immediately after the local constraint is released and the contour length of the long probe chain is preserved during the jump.[1,24] Under such assumptions, the 3D random walk or the confining tube could be considered as a freely jointed chain which moves by the "kink-jump" algorithm. This type of chain model is also termed as the Verdier−Stockmayer model.[2,65] In a short time internal Δt, an internal bead i of the freely jointed chain executes a jump with a probability $w\Delta t$ by exchanging the two bond vectors $\mathbf{b}_i$ and $\mathbf{b}_{i-1}$ connected to it while an end bead makes jump with the same probability by rotating the bond connecting it to the neighboring bead of the chain through a random uniformly distributed angle. The freely jointed chain in the continuum with kink-jump motion and no excluded volume effect is an exact equivalent to the Rouse chain model.[2,65] In the CR Rouse motion model, the characteristic jump time of a tube segment is assumed to be the terminal time of the matrix chains.[18] For a freely jointed chain this corresponds to a mean jump rate of the beads of $w = 1/\tau_{d,S}$. However, the broad distribution of the relaxation rates has been indicated to play an important role in determining the dynamics of the long probe chains. Thus, we adopt the spectrum of the relaxation (jump) rates used by Rubinstein and Colby in their self-consistent theoretical model,[14] which was derived from the stress relaxation function proposed by Doi for considering the contour length fluctuation effects,[12]

$$P(w) = \begin{cases} 0 & w < \dfrac{1}{\tau_S^{rep}(1 - \nu/\sqrt{Z_S})^2} \\ \dfrac{1}{2\sqrt{\tau_S^{rep}}} w^{-3/2} & \dfrac{1}{\tau_S^{rep}(1 - \nu/\sqrt{Z_S})^2} < w < \dfrac{Z_S}{\nu^2\tau_S^{rep}} \\ \dfrac{1}{2}\left(\dfrac{\nu^2}{Z_S\tau_S^{rep}}\right)^{1/4} w^{-5/4} & w > \dfrac{Z_S}{\nu^2\tau_S^{rep}} \end{cases} \tag{21}$$

where τ_S^{rep} and Z_S are the pure reptation time and number of entanglements of the short matrix chain, respectively, and ν is a numerical prefactor and is taken to be 1.[14] The influence of constraint release effect on the relaxation of the matrix chains is not considered in deriving eq 21. Each bead of the freely jointed chain representing the tube is initially assigned a jump rate w randomly taken from the probability distribution of eq 21. The jump of the bead according to w is controlled by a Metropolis algorithm. At each time step of the simulation run, a random number between 0 and 1 is generated from a uniform distribution for the bead and is compared with the value of $w\Delta t$. If this random number is smaller than $w\Delta t$, the bead performs a kink-jump and simultaneously updates its jump rate by taking a new value of w from $P(w)$; otherwise, it will remain in the previous position, unless being evacuated by the Rouse chain reptation. The values of the assigned jump rates are kept to be $w \le 1/\tau_e$ to meet the physical condition that the lifetime of a topological constraint is longer than the equilibration time τ_e. The update of the jump rate after each constraint release event is more realistic than the use of fixed value of w for each bead after the initial assignment.[14]

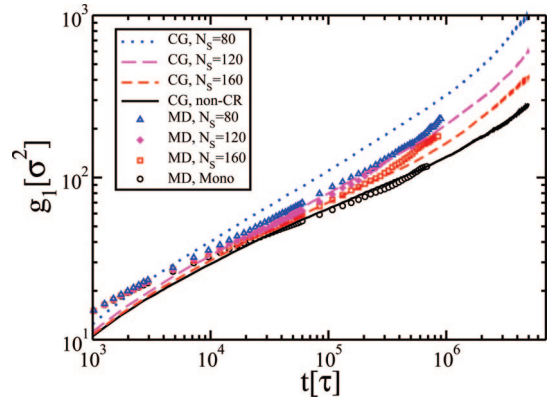

Figure 12. Simulation results (lines) of the coarse-grained Rouse chain model for the mean square monomer displacement $g_{1,R}$ of the probe chains as a function of time. The symbols are the standard MD simulation results for $g_{1,L}(t)$ obtained for binary blends with long chain length $N_L = 350$ and long chain segment fraction $n_L = 0.15$.

The parameters we used in the CG simulations are as following.[39] The Kuhn segment length of the semiflexible linear chain used in our MD simulations is $l_k = 3.34\sigma$ and the tube diameter $d_T^p = 8.6\sigma$.[10] Thus the long probe chain with $N_L = 350$ monomers has $N_K = N_L l/l_k = 102$ Kuhn steps. For the corresponding coarse-grained 1D bead-spring Rouse chain with N_R springs, each spring corresponds to $N_{K,R} = N_K/N_R$ Kuhn segments, which gives a spring constant $K_R = 3k_BT/(N_{K,R}l_k^2)$. The friction coefficient per Rouse bead is $\zeta_R = N_{K,R}\zeta_k$ with the friction coefficient per Kuhn segment $\zeta_k = 171.6k_BT\tau\sigma^{-2}$ estimated from the relation of $\zeta_k = (N_L/N_K)\zeta^e = (N_L/N_K)(k_BT/Wb^2)$ and the value of $W = 6.24 \times 10^{-3}\tau^{-1}$. In accordance with the original work of Rubinstein and Colby,[14] we use the pure reptation time of the short matrix chains, $\tau_S^{rep} = 3\tau_e(N_S/N'_e)^3 \approx 0.74N_S^3\tau$ (see section 3.2.1), in the jump rate distribution function of eq 21. The equations of motion of the Rouse beads (eqs 18, 19, and 20) are integrated with the simple Euler forward difference scheme with a time step $\Delta t = 0.1\tau$. Simulations were performed on an ensemble of 100 individual Rouse chains with each chain having $N_R = 60$ beads. The systems were first equilibrated for a time period of $2 \times 10^6\tau$, and the results were then collected from a product run of $8 \times 10^6\tau$. The mean square bead displacement, $g_{1,R}(t)$, was calculated by averaging over the innermost five beads of the Rouse chains. We have monitored the distribution $p(w)$ of the jump rates assigned to the beads of the freely jointed chains in the whole ensemble, and eq 21 was found to be well preserved in each simulation run.

Figure 12 shows the CG simulation results for $g_{1,R}(t)$ obtained from systems representing binary blends of long probe chains with $N_L = 350$ monomers diluted in matrices of different short chain lengths, together with the corresponding MD simulation data. In the monodisperse case, the CG simulations with and without consideration of the constraint release effect provide

very close results due to the long waiting time of the kink jumps, thus only the data with non-CR effect are presented. As has been observed in the previous work,[39] the CG results in this case agree very well with the MD simulation data at time scales larger than τ_e, showing the negligible constraint release effect in the monodisperse melts of sufficiently long chains. The discrepancy between the two set of data at shorter times $t < \tau_e$ results from the coarse-graining of the small length scales in the 1D Rouse chain model.[39] In case of binary blends, Figure 12 demonstrates that the coarse-grained simulation model incorporating kink-jump motions of the tube segments is able to capture the correct physical picture of constraint release effect on the dynamics of the long probe chains. The decrease of the relaxation time of the shorter matrix chains leads to higher jump rates of the long-chain tube segments, and thus accelerates the dynamic relaxation of the long chains. The predictions of the CG simulations for $g_{1,R}(t)$ are qualitatively consistent with the corresponding MD simulation data. The quantitative difference between these two cases could be related to some approximations used in the coarse-grained simulation algorithm. First of all, the jump rate distribution eq 21 is based on a single-chain stress relaxation function which itself is an approximate formula developed for describing the effect of contour length fluctuations.[12,14] The constraint release effect on the relaxation of the matrix chains themselves has been neglected. Thus this distribution function should in principle work more properly for the systems with sufficiently long matrix chains. This is elucidated by the rather close CG and MD results for binary blends with matrix chain length $N_S \geq 120$. The most appropriate function for describing the relaxation rate distribution of the topological constraints is, however, still an open question, as implied in section 3.3. The other assumptions, which are frequently used in the CR Rouse motion theories[14,15,18] and are thus implemented in the current coarse-grained model, include that the departure of one matrix chain could lead to the release of one topological constraint and the effective jump distance of the tube segment caused by one CR event is of the size of the entire tube segment. Since one entanglement is created by the effective packing of many chains, the escape of one matrix chain should not be sufficient to free an entire tube segment.[15] The use of these assumptions can lead to an overestimation of the contribution from constraint release effects, especially for binary blends with smaller N_S values where the shorter matrix chains have a higher frequency to enter and depart from the tube region of the probe chains. Moreover, the tube Rouse motion behavior is assumed to be still valid in the CG simulations for systems with $N_S \leq 80$. Figure 8, however, shows that there is a departure from CR Rouse theory at $N_S = 80$, because of a cross-over to unentangled chain motion represented by the dotted line. As a result, higher monomer diffusion rates are predicted by the CG model for the probe chains in matrices of shorter chain lengths $N_S \leq 80$, see Figure 12. The long-chain diffusion coefficients D_L calculated in this crossover region are also found to follow a N_S dependence similar to that predicted by eqs 15 and 16 (thick solid and dotted-dashed curves in Figure 8), larger than the corresponding MD simulation values. To examine the quantitative behavior of the CG model in the CR Rouse dominant regime will require MD simulation data obtained from binary blends with much longer probe chains. Despite that the coarse-grained algorithm still needs to be refined to yield results perfectly matching the fine scale molecular dynamics simulation data, it is shown to be a very promising tool for testing the theoretical models developed for describing the constraint release effects in polydisperse polymer melts. Good agreement between the CG and MD simulation data could be expected with the improved understanding of the constraint release mechanism.

4. Conclusions

In this paper, we report extensive molecular dynamics simulation studies of the dynamics of entangled binary blends consisting of long probe chains diluted in a short-chain matrix. The long probe chains of length $N_L \geq 350$ have $Z_L = N_L/N_e^P > 15$ entanglements per chain, calculated from the entanglement length of $N_e^P = 23$, estimated for the semiflexible chain model used in the current work.[10] The constraint release effect in the binary blends is investigated by systematically reducing the short chain length N_S from the monodisperse case of $N_S = N_L$ to slightly above one entanglement length. The Struglinski−Graessley parameter, $r_{SG} \equiv N_L N_e^2/N_S^3$, is correspondingly varied over more than three decades, which is large enough to encompass the crossover from the chain reptation regime to tube Rouse motion regime of the long probe chains. The realism of the simulations is validated by the agreement of prediction of the single-chain dynamic structure factor, $S(k,t)$, of the probe chains with experimental neutron spin echo data from literature.[26] In binary blends, the constraint release effect leads to faster decay of $S(k,t)$ with decreasing matrix chain length.

We then investigated the diffusion properties of the binary blends by calculating the mean square displacements of the individual monomers, $g_{1(2)}(t)$, and the center of mass of the whole chain, $g_3(t)$, as well as the chain diffusion coefficient, D. As expected, at short time scales below the equilibration time τ_e, the diffusion curves $g_{1(2,3),L}(t)$ of the long probe chains in all binary blends fall exactly on top of each other. However, immediately after τ_e, $g_{1(2),L}(t)[g_{3,L}(t)]$ rises above the $g_{1(2),L}(t) \propto t^{1/4}[g_{3,L}(t) \propto t^{1/2}]$ behavior of pure long-chain melts and shows instead power law scaling, $g_L(t) \propto t^x$, with the value of the exponent x increasing with decrease in the matrix chain length in the intermediate time regime below the Rouse time $\tau_{R,L}$ of the probe chains. These results are not consistent with the simple constraint-release Rouse picture, wherein the contour length fluctuations of the matrix chains are neglected and the constraint release is assumed to be dominated by a constraint release time scale of order $\tau_{d,S}$, the reptation time of the short chains. Instead, the results suggest the existence of a very broad distribution of constraint lifetimes. This conclusion is supported by a microscopic analysis of the lifetime of residence of short chains inside the "tube" surrounding the long chain. In the analysis, short chains having $N_e^P/2$ monomers within a radius of $d_T/2$ of the primitive path of the long chain are said to be in the tube of that long chain, where d_T is the tube diameter. The Rouse-like tube reorganization behavior predicted by the constraint release Rouse model is only observed in the monomer diffusion at large time scales close and beyond $\tau_{R,L}$ and in the diffusion of the center of mass of the whole chain at $t > \tau_{d,S}$. In these cases, the dynamics of the probe chains is less sensitive to the distribution of the disentanglement rates.

The diffusion coefficient of the semiflexible probe chains obtained in our simulations demonstrates a weaker N_S dependence than observed in the tracer diffusion coefficient experiments performed on binary blends of linear polystyrenes with a comparable number of entanglement per probe chain[21] but is consistent with the experimental data achieved in the blends of linear poly(propylene oxide).[32] This suggests that the number of entanglements per chain is not the only factor affecting the dynamics of binary blends but that the influence of other molecular factors, such as the chain stiffness or free volume changes with molecular weight, should also be taken into account.

We have improved the coarse-grained simulation model developed by Zhou and Larson[39] by incorporating the kink-jump motions of the tube segments according to a theoretically proposed probability distribution of the jump rates.[14] This algorithm has been shown to provide predictions for the dynamic

relaxation of the long probe chains in binary blends qualitatively, but not quantitatively, consistent with fine-scale molecular dynamics simulations. Further progress in understanding constraint release processes can no doubt be obtained from longer simulations with longer, and more flexible, polymer chains.

Acknowledgment. We gratefully acknowledge the financial support provided by the donors of the Petroleum Research Fund, administered by the American Chemical Society, through grant number ACS PRF # 45882-AC7, which partly funded this research. We also acknowledge support from NSF under grant DMR 0604965. Any opinions, findings, and conclusions or recommendations expressed in this material are those of the authors and do not necessarily reflect the views of the National Science Foundation (NSF). Helpful discussions with Dr. Alexei E. Likhtman and Dr. William W. Graessley are gratefully acknowledged.

References and Notes

(1) Graessley, W. W. *Adv. Polym. Sci.* **1982**, *47*, 67–117.
(2) Doi, M.; Edwards, S. F. *The theory of polymer dynamics*, 1st ed.; Claredon Press: Oxford, 1988.
(3) McLeish, T. C. B. *Adv. Phys.* **2002**, *51*, 1379–1527.
(4) de Gennes, P. G. *J. Chem. Phys.* **1971**, *55*, 572–579.
(5) Rubinstein, M.; Colby, R. H. *Polymer Physics*, 1st ed.; Oxford University Press: New York, 2003.
(6) Wischnewski, A.; Monkenbusch, M.; Willner, L.; Richter, D.; Kali, G. *Phys. Rev. Lett.* **2003**, *90*, 058302.
(7) Kremer, K.; Grest, G. S.; Carmesin, I. *Phys. Rev. Lett.* **1988**, *61*, 566–569.
(8) Kremer, K.; Grest, G. S. *J. Chem. Phys.* **1990**, *92*, 5057–5086.
(9) Pütz, M.; Kremer, K.; Grest, G. S. *Europhys. Lett.* **2000**, *49*, 735–741.
(10) Everaers, R.; Sukumaran, S. K.; Grest, G. S.; Svaneborg, C.; Kremer, A. S. A. *Science* **2004**, *303*, 823–826.
(11) Zhou, Q.; Larson, R. G. *Macromolecules* **2006**, *39*, 6737–6743.
(12) Doi, M. *J. Polym. Sci., Polym. Lett. Ed.* **1981**, *19*, 265–273.
(13) Milner, S. T.; McLeish, T. C. B. *Phys. Rev. Lett.* **1998**, *81*, 725–728.
(14) Rubinstein, M.; Colby, R. H. *J. Chem. Phys.* **1988**, *89*, 5291–5306.
(15) Likhtman, A. E.; McLeish, T. C. B. *Macromolecules* **2002**, *35*, 6332–6343.
(16) Marrucci, G. *J. Polym. Sci., Part B: Polym. Phys.* **1985**, *23*, 159–177.
(17) Doi, M.; Graessley, W. W.; Helfand, E.; Pearson, D. S. *Macromolecules* **1987**, *20*, 1900–1906.
(18) Viovy, J. L.; Rubinstein, M.; Colby, R. H. *Macromolecules* **1991**, *24*, 3587–3596.
(19) Park, S. J.; Larson, R. G. *Macromolecules* **2004**, *37*, 597–604.
(20) Green, P. F.; Mills, P. J.; Palmstrom, C. J.; Mayer, J. W.; Kramer, E. J. *Phys. Rev. Lett.* **1984**, *53*, 2145–2148.
(21) Green, P. F.; Kramer, E. J. *Macromolecules* **1986**, *19*, 1108–1114.
(22) Watanabe, H.; Kotaka, T. *Macromolecules* **1984**, *17*, 2316–2325.
(23) Watanabe, H.; Yamazaki, M.; Yoshida, H.; Kotaka, T. *Macromolecules* **1991**, *24*, 5573–5581.
(24) Watanabe, H. *Prog. Polym. Sci.* **1999**, *24*, 1253–1403.
(25) Watanabe, H.; Ishida, S.; Matsumiya, Y.; Inoue, T. *Macromolecules* **2004**, *37*, 6619–6631.
(26) Zamponi, M.; Wischnewski, A.; Monkenbusch, M.; Willner, L.; Richter, D.; Likhtman, A. E.; Kali, G.; Farago, B. *Phys. Rev. Lett.* **2006**, *96*, 238302.
(27) von Meerwall, E. D.; Dirama, N.; Mattice, W. L. *Macromolecules* **2007**, *40*, 3970–3976.
(28) Klein, J. *Macromolecules* **1978**, *11*, 852–858.
(29) Daoud, M.; deGennes, P. G. *J. Polym. Sci., Part B: Polym. Phys.* **1979**, *17*, 1971–1981.
(30) Wang, S. *J. Polym.Sci., Part B: Polym. Phys.* **2003**, *41*, 1589–1604.
(31) Smith, B. A.; Samulski, E. T.; Yu, L. P.; Winnik, M. A. *Phys. Rev. Lett.* **1984**, *52*, 45–48.
(32) Smith, B. A.; Samulski, E. T.; Yu, L. P.; Winnik, M. A. *Macromolecules* **1985**, *18*, 1901–1905.
(33) Pearson, D. S.; Strate, G. V.; von Meerwall, E.; Schilling, F. C. *Macromolecules* **1987**, *20*, 1133–1141.
(34) Struglinski, M. J.; Graessley, W. W. *Macromolecules* **1985**, *18*, 2630–2643.
(35) Park, S. J.; Larson, R. G. *J. Rheol.* **2006**, *50*, 21–39.
(36) Likhtman, A. E. *Macromolecules* **2005**, *38*, 6128–6139.
(37) McLeish, T. C. B. *Europhys. Lett.* **1988**, *6*, 511–516.
(38) Larson, R. G. *Macromolecules* **2001**, *34*, 4556–4571.
(39) Zhou, Q.; Larson, R. G. *Macromolecules* **2007**, *40*, 3443–3449.
(40) Kolinski, A.; Skolnick, J.; Yaris, R. *J. Chem. Phys.* **1987**, *86*, 7174–7180.
(41) Baschnagel, J.; Paul, W.; Binder, V. T. K. *Macromolecules* **1998**, *31*, 3856–3867.
(42) Barsky, S. *J. Chem. Phys.* **2000**, *112*, 3450–3456.
(43) Lin, H.; Mattice, W. L.; von Meerwall, E. D. *Macromolecules* **2007**, *40*, 959–966.
(44) Rathgeber, S.; Willner, L.; Richter, D.; Brulet, A.; Farago, B.; Appel, M.; Fleischer, G. *J. Chem. Phys.* **1999**, *110*, 10171–10187.
(45) Pearson, D. S.; Fetters, L. J.; Graessley, W. W.; Strate, G. V.; von Meerwall, E. *Macromolecules* **1994**, *27*, 711–719.
(46) von Meerwall, E.; Feick, E. J.; Ozisik, R.; Mattice, W. L. *J. Chem. Phys.* **1999**, *111*, 750–757.
(47) Picu, R. C.; Rakshit, A. *J. Chem. Phys.* **2007**, *127*, 144909.
(48) Auhl, R.; Everaers, R.; Grest, G. S.; Kremer, K.; Plimpton, S. J. *J. Chem. Phys.* **2003**, *119*, 12718–12728.
(49) Schleger, P.; Farago, B.; Lartigue, C.; Kollmar, A.; Richter, D. *Phys. Rev. Lett.* **1998**, *81*, 124–127.
(50) Zamponi, M.; Monkenbusch, M.; Willner, L.; Wischnewski, A.; Farago, B.; Richter, D. *Europhys. Lett.* **2005**, *72*, 1039–1044.
(51) Wischnewski, A.; Richter, D. *Europhys. Lett.* **2000**, *52*, 719–720.
(52) DeGennes, P. G. *J. Phys. (Paris)* **1981**, *42*, 735–740.
(53) Wischnewski, A.; Monkenbusch, M.; Willner, L.; Richter, D.; Likhtman, A. E.; McLeish, T. C. B.; Farago, B. *Phys. Rev. Lett.* **2002**, *88*, 058301.
(54) Pütz, M.; Kremer, K.; Grest, G. S. *Europhys. Lett.* **2000**, *52*, 721–722.
(55) Carella, J. M.; Graessley, W. W.; Fetters, L. J. *Macromolecules* **1984**, *17*, 2775–2786.
(56) Watanabe, H.; Sakamoto, T.; Kotaka, T. *Macromolecules* **1985**, *18*, 1436–1442.
(57) Watanabe, H.; Urakawa, O.; Kotaka, T. *Macromolecules* **1994**, *27*, 3525–3536.
(58) Klein, J. *Macromolecules* **1986**, *19*, 105–118.
(59) Fetters, L. J.; Lohse, D. J.; Graessley, W. W. *J. Polym. Sci., Part B:, Polym. Phys.* **1999**, *37*, 1023–1033.
(60) von Seggern, J.; Klotz, S.; Cantow, H. J. *Macromolecules* **1991**, *24*, 3300–3303.
(61) Sawada, T.; Qiao, X.; Watanabe, H. *J. Soc. Rheol., Jpn.* **2007**, *35*, 11–20.
(62) Likhtman, A. E.; Sukumaran, S. K.; Ramirez, J. *Macromolecules* **2007**, 40.
(63) Zhou, Q.; Larson, R. G. *Macromolecules* **2005**, *38*, 5761–5765.
(64) Milner, S. T. *Macromolecules* **2005**, *38*, 4929–4939.
(65) Verdier, P. H.; Stockmayer, W. H. *J. Chem. Phys.* **1962**, *36*, 227–235.

MA800680B